Glein C. R., Postberg F., and Vance S. D. (2018) The geochemistry of Enceladus: Composition and controls. In *Enceladus and the Icy Moons of Saturn* (P. M. Schenk et al., eds.), pp. 39–56. Univ. of Arizona, Tucson, DOI: 10.2458/azu_uapress_9780816537075-ch003.

The Geochemistry of Enceladus: Composition and Controls

C. R. Glein
Southwest Research Institute

F. Postberg
University of Heidelberg

S. D. Vance
NASA Jet Propulsion Laboratory/California Institute of Technology

Enceladus is the first world beyond Earth for which we have diagnostic observational data concerning the composition of an extant ocean. The abundances of chemical species in the plume of Enceladus, which is sourced by the ocean, provide valuable constraints on the temperature, major ion composition, pH, and reduction-oxidation (redox) chemistry of its ocean. The pressure profile is determined by the internal structure of the moon, which also constrains temperatures in Enceladus' rocky core. The data indicate that the ocean is a relatively alkaline and reduced solution of dissolved sodium, chloride, and bicarbonate/carbonate ions just below the freezing point of pure water. Observations of silica nanoparticles and molecular hydrogen from Enceladus can be explained in terms of hydrothermal sources. We present a model in which the dissolution of quartz in hot water yields high concentrations of silica, and reduced rocks tidally heated in the presence of water supply abundant hydrogen. Future studies should seek to address many of the geochemical questions raised by the Cassini era of Enceladus exploration.

1. ENCELADUS AS A GATEWAY TO EXTRATERRESTRIAL OCEANOGRAPHY

Numerous lines of evidence made possible by the Cassini-Huygens mission (*Porco et al.,* 2006, 2014; *Spencer et al.,* 2006; *Collins and Goodman,* 2007; *Nimmo et al.,* 2007; *Zolotov,* 2007; *Glein et al.,* 2008; *Schmidt et al.,* 2008; *Tobie et al.,* 2008; *Postberg et al.,* 2009, 2011; *Waite et al.,* 2009, 2017; *Glein and Shock,* 2010; *Ingersoll and Pankine,* 2010; *Patthoff and Kattenhorn,* 2011; *Běhounková et al.,* 2012; *Matson et al.,* 2012; *Iess et al.,* 2014; *Bouquet et al.,* 2015; *Hsu et al.,* 2015; *McKinnon,* 2015; *Travis and Schubert,* 2015; *Beuthe et al.,* 2016; Čadek et al., 2016; *Ingersoll and Nakajima,* 2016; *Kite and Rubin,* 2016; *Nakajima and Ingersoll,* 2016; *Thomas et al.,* 2016; *Choblet et al.,* 2017; see also chapters by Hemingway et al. and Spencer et al. in this volume) support the paradigm that Saturn's moon, Enceladus, has a global subsurface ocean of liquid water, which erupts into space forming a south polar plume of gases and ice grains. From a geochemical perspective, what is most remarkable about Enceladus is that its plume provides access to the chemical composition of its ocean. The relative ease of obtaining constraints on the geochemistry of the subsurface of Enceladus is unprecedented in the field of planetary science, where detailed information on composition usually necessitates landers.

Why might one be interested in the geochemistry of Enceladus? First, it is of broad interest because the composition of the environment imposes boundary conditions on the possible origin, evolution, and persistence of life (*McKay et al.,* 2008). Second, the accessibility of its ocean enables Enceladus to serve as a model for the geochemistry of oceans inside other icy worlds, such as Ganymede (*Vance et al.,* 2014), Callisto, Mimas, Dione, Titan (*Glein,* 2015), Triton (*Shock and McKinnon,* 1993), and Pluto (*Neveu et al.,* 2015). Third, knowledge of the geochemistry of Enceladus allows us to frame the subject of aqueous geochemistry in a more universal context. This will help us to better understand the processes that led to similarities and differences in the observed compositions of water-bearing bodies across the solar system, including Earth (*Lowenstein et al.,* 2014; *German and Seyfried,* 2014), Mars (*Ehlmann et al.,* 2013; *Niles et al.,* 2013), carbonaceous chondrite parent bodies (*Brearley,* 2006), Ceres (*Zolotov,* 2017), and Europa (*Zolotov and Kargel,* 2009; *Vance et al.,* 2016). Fourth, this is new science; the thrill of exploration motivates the burgeoning field of extraterrestrial chemical oceanography.

In this chapter, we examine key aspects of the geochemistry of Enceladus. The chapter contains a mixture of review material and more refined interpretations. We begin with an overview of the relevant observational data (see section 2). Then, we organize our discussion of enceladean geochemistry

into two parts: marine geochemistry (see section 3) and hydrothermal geochemistry (see section 4). Figure 1 shows the locations of these types of geochemistry with respect to the vertical structure of Enceladus. In reality, the boundaries may not be sharp. Our goals in these discussions are to (1) introduce some of the basic concepts of geochemistry that are useful for interpreting chemical data from Enceladus, and (2) present contemporary models for the compositions of the ocean and suspected hydrothermal fluids. We conclude this chapter with a set of critical questions to take us from Cassini to the next era of exploration (see section 5).

2. CONSTRAINTS FROM PLUME COMPOSITION

Because the plume of Enceladus is sourced from a liquid water ocean (see section 1), the plume's composition can provide insights into the geochemistry of Enceladus' ocean and deeper hydrothermal fluids. The Cosmic Dust Analyzer (CDA) and the Ion and Neutral Mass Spectrometer (INMS) were the primary instruments onboard the Cassini spacecraft that measured the composition of the plume (see the chapter by Postberg et al. in this volume). *In situ* measurements were performed when the spacecraft flew through the plume, or sampled Saturn's E ring, which is maintained by the delivery of plume materials (*Haff et al.,* 1983; see the chapter by Kempf et al. in this volume).

The CDA instrument discovered that the plume contains three compositionally distinct populations of ice grains (*Postberg et al.,* 2008, 2009, 2011, 2018). Type I is nearly pure water ice, Type II contains organic compounds, and Type III is rich in salts. The largest mass line in CDA spectra of Type III grains is from Na^+; smaller mass lines from K^+, and sodium clusters with OH^-, Cl^-, and/or CO_3^{-2}, were observed (*Postberg et al.,* 2009). The salt-rich ice grains are thought to form by flash freezing of ocean water. The large abundance of Na in these grains is indicative of extensive water-rock interaction (*Zolotov,* 2007), consistent with the presence of a rocky core with a low density (*Iess et al.,* 2014; *McKinnon,* 2015; see the chapter by Hemingway et al. in this volume), resulting from silicate hydration.

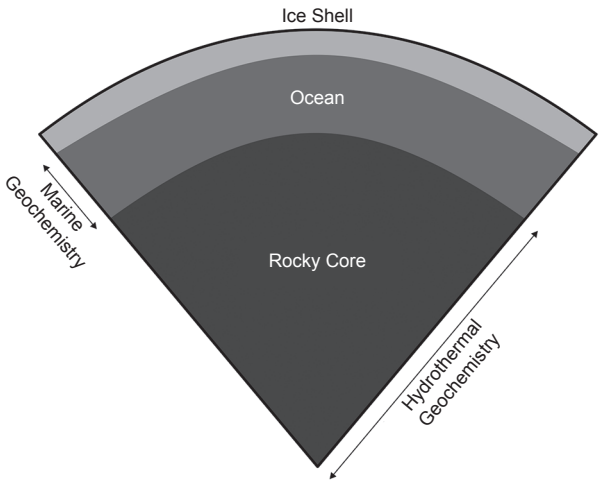

Fig. 1. The two general categories of geochemical processes shown in a schematic cross section of Enceladus.

Postberg et al. (2009) used a laser to generate gaseous ions from solutions containing NaCl and $NaHCO_3$ or Na_2CO_3. Laser ionization in the laboratory was meant to serve as a proxy for impact ionization in the CDA instrument. It was found that CDA spectra of salt-rich ice grains can be reproduced from solutions containing 0.05–0.2 mol NaCl per kg H_2O and 2–5 times more chloride than bicarbonate or carbonate (throughout this chapter, molality (mol/kg H_2O) is the preferred unit for the concentrations of aqueous species). There is currently ambiguity as to whether HCO_3^- or CO_3^{-2} is predominant in the ocean source of the plume, because solutions containing either of these species are able to reproduce a mass peak attributed to $(Na_2CO_3)Na^+$ (*Postberg et al.,* 2009). The salt composition derived by *Postberg et al.* (2009) is summarized in Table 1.

The CDA detected silicon-rich, nanometer-scale particles escaping from the saturnian system, during the approach of the spacecraft to Saturn (*Kempf et al.,* 2005). These particles are thought to originate as inclusions in Type II or III E-ring ice grains, and then be released from the grains by plasma-sputtering erosion (*Hsu et al.,* 2011). Therefore, their source is inferred to be the plume of Enceladus. The Si-rich stream particles are poor in metal cations, which implies that they are composed of nearly pure silica (SiO_2). It is difficult to determine the concentration of silica in ocean-derived ice grains, as silica was not measured in the plume or E ring. The current best estimate is a SiO_2 concentration of ~150–3900 ppm by mass, based on the dynamical modeling of *Hsu et al.* (2015).

The INMS made measurements of gas molecules in the plume, using both closed- and open-source modes of operation. The former mode provides greater sensitivity, but some species undergo chemical reactions inside the instrument before they are able to reach the detector. In open-source mode, collisions and thus chemical reactions of plume materials are minimized. The initial set of closed-source data revealed that the most abundant plume constituent is water vapor (*Waite et al.,* 2006), consistent with observations by the Ultraviolet Imaging Spectrograph (UVIS) (*Hansen et al.,* 2006). Subsequent INMS measurements showed that the detected composition depends on the flyby velocity, indicative of reactions of certain plume materials (e.g., organic compounds) induced by high-energy impacts of ice grains on the walls of the instrument (*Waite et al.,* 2009). Hydrogen

TABLE 1. Major composition of salt-rich ice grains in Enceladus' plume.

Constituent	Concentration (mol/kg H_2O)
NaCl	0.05–0.2
$NaHCO_3 + Na_2CO_3$	0.01–0.1
KCl	$(0.5–2) \times 10^{-3}$

Data from *Postberg et al.* (2009, 2011).

gas in the closed source was inferred to be produced by interactions between water molecules and titanium metal in the INMS antechamber (*Waite et al.,* 2009, 2017).

The final set of measurements, made in open-source mode, provide the most reliable discrimination between the true composition vs. the impact-modified composition (*Waite et al.,* 2017). These data indicate the presence of H_2O, H_2, and CO_2. The identification of CO_2 in the plume gas is further supported by observations of CO_2 in the tiger stripes region on the surface of Enceladus by the Visible and Infrared Mapping Spectrometer (VIMS) (*Brown et al.,* 2006). No mass-28 species were detected in open-source mode, consistent with the lack of detection of CO (*Hansen et al.,* 2008) and N_2 (*Hansen et al.,* 2011) by UVIS. However, a mass-28 species was detected using the closed source (*Waite et al.,* 2006, 2009).

The discrepancy between the open- and closed-source data with regards to the detection of mass 28 (*Waite et al.,* 2017) implies that a closed-source detection may be considered tentative if an open-source measurement was not made. Two major species fall into this category: NH_3 and CH_4. Observations of NH_3 on Enceladus' surface are presently equivocal (*Brown et al.,* 2006; *Hendrix et al.,* 2010), but the discovery of N^+ in Saturn's inner magnetosphere by the Cassini Plasma Spectrometer (CAPS) suggests that plume NH_3 may be the parent species (*Smith et al.,* 2008; see the chapter by Postberg et al. in this volume). This supports the identification of NH_3 in the plume. For CH_4, we are not aware of any additional observational evidence for its presence at Enceladus. The gas composition derived by *Waite et al.* (2017) is summarized in Table 2.

3. MARINE GEOCHEMISTRY

3.1. Pressure and Temperature in the Ocean

Pressures in the ocean of Enceladus can be estimated from models of the internal structure of the satellite. These models are constrained by Cassini measurements of gravity, topography, and libration (*Iess et al.,* 2014; *Thomas et al.,* 2016; see the chapter by Hemingway et al. in this volume). Here, we consider the model of *McKinnon* (2015), which has a rocky core of density 2450 kg m^{-3} and radius 190 km. We do not distinguish between the slightly different densities of water ice (~920 kg m^{-3}) and ocean water (~1030 kg m^{-3}), but instead adopt a uniform density of ρ_h = 1000 kg m^{-3} for the whole hydrosphere overlying the rocky core. For such a two-layer model in which the interior can be approximated as being in a state of hydrostatic equilibrium, the pressure (P) at radius r between the core radius and the mean surface radius (R_E = 252 km) can be computed analytically using (*Turcotte and Schubert,* 2002)

$$P = \frac{4}{3}\pi\rho_h G R_c^3 \left(\rho_c - \rho_h\right)\left(r^{-1} - R_E^{-1}\right) + \frac{2}{3}\pi G\rho_h^2\left(R_E^2 - r^2\right) \quad (1)$$

where G refers to the gravitational constant (6.674 × 10^{-11} m^3 kg^{-1} s^{-2}), R_c the radius of the core, and ρ_c its density. Figure 2 shows the pressure profile in the hydrosphere. This model yields pressures in the ocean ranging between ~2 and ~74 bar (1 bar = 0.1 MPa). Pressures are relatively low even under a deep ocean, because of Enceladus' weak gravity (the surface acceleration due to gravity g = 0.113 m s^{-2}).

Because the ocean of Enceladus is covered by water ice, its temperature ought to be affected by phase equilibrium between the ocean and ice. However, the freezing point of the ocean is depressed because the water is not pure, but contains dissolved salts that decrease the fugacity of H_2O. The fugacity can be thought of as a thermodynamically corrected partial pressure (*Anderson,* 2005). Freezing-point depression depends in general on the total concentration of solute particles but not their identities. The depression of the freezing point (ΔT_f) of the Enceladus ocean can be approximated by

$$\Delta T_f = -K_f\left(2m_{NaCl} + 2m_{NaHCO_3} + 3m_{Na_2CO_3}\right) \quad (2)$$

TABLE 2. Major composition of gases in Enceladus' plume.

Constituent	Molar Percentage
H_2O	96–99
H_2	0.4–1.4
CO_2	0.3–0.8
NH_3	0.4–1.3
CH_4	0.1–0.3

Data from *Waite et al.* (2017).

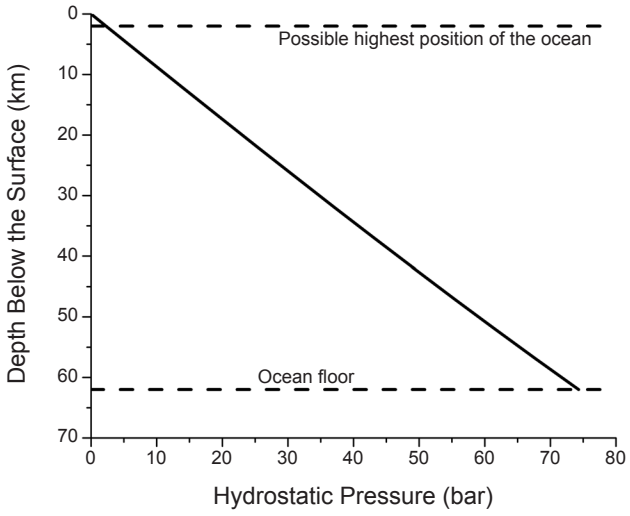

Fig. 2. Pressures in the ice shell and ocean of Enceladus based on the internal structure model of *McKinnon* (2015). The thickness of the ice shell varies with latitude and longitude, but it could be as thin as ~2 km in the south polar region (*Beuthe et al.,* 2016; Čadek et al., 2016; see the chapter by Hemingway et al. in this volume). The depth of the ocean floor follows from the core radius of ~190 km.

where K_f stands for the cryoscopic constant of water (1.86°C kg mol^{-1}), and m_i the molality of the ith salt. The coefficients (called van't Hoff factors) account for the number of ions that are released per formula unit of the corresponding salt.

Figure 3 depicts results from equation (2) for endmember salt compositions from Table 1. This plot indicates that the temperature of the ocean can be expected to be only slightly below the freezing point of pure water. The minimum temperature is about –1°C. It should be noted that ion pairing (e.g., NaCl,aq) is ignored in the present treatment, but this effect would lessen the freezing-point depression. This reinforces the conclusion that the ocean should not be much cooler than ~0°C.

An alternative frigid ocean maintained at the eutectic point of the NH_3-H_2O system (*Squyres et al.,* 1983) is implausible on Enceladus, because the plume is not rich in NH_3 (*Porco et al.,* 2006). Assuming that NH_3 is indeed present (see section 2), the NH_3/H_2O ratio in the plume gas ranges between ~0.004 and ~0.014 (Table 2). For the eutectic composition of ~35 mol% NH_3 and ~65 mol% H_2O at ~175 K, the saturation vapor pressures are predicted to be ~1 × 10^{-4} bar NH_3 and ~2 × 10^{-8} bar H_2O (*Tillner-Roth and Friend,* 1998). This corresponds to an NH_3/H_2O ratio of ~5000 in the gas phase, which is inconsistent with the data from INMS by many orders of magnitude. An analogous argument applies to methanol and other volatile antifreezes (*Waite et al.,* 2009).

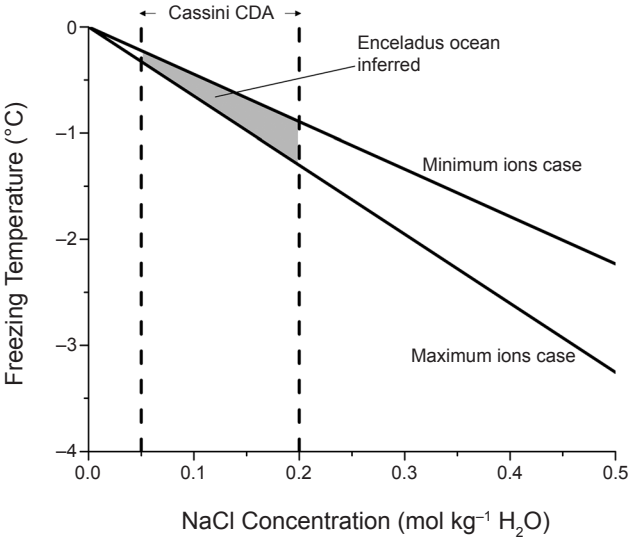

Fig. 3. Temperature of the Enceladus ocean (gray region) based on the freezing point depression of salt solutions (see section 3.1). The minimum ions case has a $NaHCO_3$/NaCl molal ratio of 0.2 (and no Na_2CO_3), while the molal ratio of Na_2CO_3/NaCl is 0.5 (with no $NaHCO_3$) in the maximum ions case (*Postberg et al.,* 2009). The dashed lines indicate the range of NaCl concentration in salt-rich plume particles (Table 1), which would be similar to that in the ocean if the water is flash frozen as a result of boiling (*Ingersoll and Nakajima,* 2016; *Nakajima and Ingersoll,* 2016).

3.2. Composition of the Ocean

3.2.1. Major ions. As a first step toward understanding the geochemistry of Enceladus' ocean, it can help to compare what we think we know about its composition to various natural waters on Earth. We compiled literature sets of representative geochemical data (Table 3) for eight terrestrial sites that may serve as physical (ice-covered) or chemical (carbonate-rich, basic pH, or reducing conditions) analogs of Enceladus' ocean. These sites are not meant to be exhaustive of all possible analogs. Rather, the intent is to introduce a group that can help us get our bearings in terms of discussing the composition of the ocean from an empirical point of view.

Our representation of seawater is the reference composition given by *Millero* (2013). Lost City is a low-temperature hydrothermal system that is located near the Mid-Atlantic Ridge (*Kelley et al.,* 2001, 2005). The fluid composition is derived from the circulation of seawater through ultramafic (magnesium- and iron-rich) rocks. This leads to hydration and oxidation (called "serpentinization") of the rocks. The Cedars is a site in northern California where ultramafic rocks are being serpentinized on a continent (*Morrill et al.,* 2013). Ronda Peridotite is another continental ultramafic site that is located in southern Spain (*Bucher et al.,* 2015). The data in Table 3 for Ronda Peridotite refer to brooks whose water has participated in extensive weathering.

Ikka Fjord is a small fjord in southwestern Greenland (*Buchardt et al.,* 1997). Towers composed of ikaite ($CaCO_3$•$6H_2O$) precipitate at the bottom of the fjord, where carbonate-rich spring water seeps into the fjord and mixes with calcium-bearing seawater. Lake Magadi is a soda lake in the East African Rift Valley in Kenya. It is a brine that is mostly covered by trona (Na_2CO_3•$NaHCO_3$•$2H_2O$). Lake Vida is a perennially ice-covered brine in the McMurdo Dry Valley of East Antarctica (*Murray et al.,* 2012). Its water chemistry may be controlled by reactions with igneous rocks in the surroundings or lake sediments, as well as freezing of water that concentrates soluble salts. Lake Untersee is another East Antarctic lake (*Wand et al.,* 1997), but it is a freshwater lake because its ice cover (~3 m) is much thinner than that over Lake Vida (~30 m).

We specify a nominal empirical composition for the Enceladus ocean to facilitate comparisons between its major ion chemistry and those of the possible analogs. We adopt a recommended pH range of 9 to 11 (see section 3.2.2). The rest of the nominal composition is as follows: (1) 0.1 molal Cl^-, (2) HCO_3^- + CO_3^{-2} concentration of 0.03 molal, (3) Na/K molal ratio of 100, and (4) H_2/CO_2 molal ratio of 1.6. These values are consistent with the data in Tables 1 and 2 (see also section 3.2.3). Speciation calculations are performed at 0°C using the thermo.com.V8.R6+ database in The Geochemist's Workbench (*Bethke,* 2008). The present model does not include Ca^{+2}, Mg^{+2}, or SO_4^{-2} as these species have not been detected in the plume or E ring. However, this does not mean that these species are absent from the ocean. We also do not consider NH_3 because it is presently unclear

TABLE 3. Geochemical properties of some potential Earth analogs of the Enceladus ocean, compared to nominal models of the latter (see section 3.2.1).

Quantity	Seawater	Lost City	The Cedars	Ronda Peridotite	Ikka Fjord	Lake Magadi	Lake Vida	Lake Untersee	Enceladus pH 9	Enceladus pH 11
T (°C)	25	90	17.2	20	4	35	–13.4	0.4	~0	~0
log a_{H_2}	–44.3	–2.0	–4.7	–45.2	–48.0	–42.8	–4.9	–48.8	–3.9	–6.8
pH	8.1	10.6	11.5	8.5	10.5	10.5	6.2	10.6	9	11
Na^+	486	511	0.94	0.17	175	6230	2090	1.98	130	154
K^+	10.6	10.8	0.01	0.005	1.66	53.5	89.2	0.08	1.30	1.54
Ca^{+2}	10.7	28.3	1.28	0.02	0.20	~0	32.4	1.04	ND	ND
Mg^{+2}	54.7	~0	0.008	3.23	~0	~0	716	0.04	ND	ND
Cl^-	566	559	0.93	0.19	22.5	2460	3510	0.87	100	100
OH^-	0.002	12.3	2.58	0.002	8e-5	0.69	5e-6	0.05	0.002	0.16
HCO_3^-	1.78	2e-4	1e-4	5.88	26.4	86.4	38.4	0.04	28.3	4.22
CO_3^{-2}	0.25	0.01	0.006	0.23	61.4	1845	0.22	0.09	1.62	25.8
SO_4^{-2}	29.3	3.31	0.001	0.04	2.74	23.6	62.9	1.43	ND	ND
I_S (molal)	0.72	0.61	0.005	0.01	0.24	8.1	4.5	0.007	0.13	0.18
Reference	*	†	‡	§	¶	**	††	‡‡	§§	§§

* *Millero* (2013).
† *Seyfried et al.* (2015).
‡ *Morrill et al.* (2013).
§ *Bucher et al.* (2015).
¶ *Buchardt et al.* (2001).
** *Jones et al.* (1977).
†† *Murray et al.* (2012).
‡‡ *Wand et al.* (1997).
§§ This work.

Oxidation state is expressed in terms of the activity of H_2 (a_{H_2}). Values for the aqueous species are stoichiometric concentrations (mmoles per kilogram of water) that include the free ion and ion pairs. The ionic strength is given as the stoichiometric ionic strength (I_S). ND means not detected.

how the plume abundance of NH_3 (Table 2) translates to an ocean concentration. Because NH_3 is relatively non-volatile, it probably freezes out during transport and thus does not exhibit conservative behavior between the ocean and plume.

The concentrations of major ions in Table 3 reveal similarities and differences between the natural waters on Earth and Enceladus' ocean. Seawater is similar to Enceladus' ocean in terms of being dominated by NaCl. However, seawater is poorer in carbonate species, and may be richer in Mg^{+2} and SO_4^{-2} than the Enceladus ocean if the lack of detection of these species by CDA argues against the ocean containing more than ~10 mmolal $MgSO_4$. The serpentinization systems at Lost City and the Cedars both have relatively high concentrations of dissolved calcium hydroxide. This drives a decrease in the concentrations of carbonate species in these systems, unlike the case of Enceladus. Ronda Peridotite also appears to differ from the Enceladus ocean, as the former is dominated by Mg^{+2} and HCO_3^-. In contrast, both Ikka Fjord and Lake Magadi seem similar to Enceladus' ocean in terms of being rich in Na^+, Cl^-, and carbonate species. Lake Vida may have a larger enrichment in Mg^{+2} than the ocean of Enceladus, if it is assumed that this species has a concentration below ~10 mmolal in the latter. Finally, the large relative contributions from Ca^{+2} and SO_4^{-2} to the ion chemistry of Lake Untersee may represent a key difference between this environment and Enceladus' ocean.

We also observe that some of the potential analogs are similar to the models of the Enceladus ocean with respect to ionic strength (an indicator of total salt content), while others are dramatically different (Table 3). Both seawater and Lost City fluid (derived from seawater) are modestly higher in ionic strength than modeled ocean water on Enceladus, whereas rainwater-derived fluids at the Cedars and Ronda Peridotite are markedly lower in ionic strength. Ikka Fjord presents an interesting case that appears to have a similar ionic strength as the ocean of Enceladus. It is apparent that waters from both Lake Magadi and Lake Vida are much higher in ionic strength than the Enceladus ocean (Table 3). Conversely, the low ionic strength of Lake Untersee makes this body of glacial meltwater much "fresher" than the ocean of Enceladus.

Based on the preceding comparisons, Ikka Fjord and seawater may be the closest analogs of the Enceladus ocean out of the eight cases considered, with respect to the composition of major ions. We caution that these analogs are not perfect matches to Enceladus (nor should we expect them to be given the different geological contexts). But between the two of them, they adequately mirror the dominant Na-Cl-HCO_3/CO_3 chemistry of the Enceladus ocean.

3.2.2. pH. The pH of an aqueous solution is given by the following equation

$$\mathrm{pH} = -\log\left(a_{H^+}\right) \tag{3}$$

where a_{H^+} stands for the activity of the hydrogen ion [the standard state for aqueous species, which defines an activity

of unity, is a hypothetical one molal solution referenced to infinite dilution at any temperature and pressure (*Anderson,* 2005)]. A solution with a low pH is acidic because the activity of H^+ is high. Self-ionization of water relates the acidity and basicity of the solution via

$$H_2O, aq \leftrightarrow H^+, aq + OH^-, aq \quad (4)$$

which has an equilibrium constant

$$K_w = \frac{a_{H^+} a_{OH^-}}{a_{H_2O}} = 10^{-14.94} \text{ at 0°C and 1 bar} \quad (5)$$

The activities (a) of H^+ and OH^- are inversely related. The activity of H_2O is usually close to unity (the pure standard state) in natural waters, with the exception of brines. From equation (5), it can be deduced that a basic solution with a high activity of OH^- must have a low activity of H^+ and thus a high pH. A solution is said to be neutral if the activities of H^+ and OH^- are equal. The neutral pH at 0°C is ~7.5.

The pH is generally the most important compositional variable in aquatic systems. It has a powerful influence on the geochemical behavior of almost all the elements, except for the noble gases, the alkali metals, and the halogens. The pH governs the speciation of many systems, as species interconvert by releasing or taking up H^+. The carbonate system provides a classic example that is relevant to the geochemistry of Enceladus. The chief equilibria are

$$CO_2, aq + H_2O, aq \leftrightarrow H^+, aq + HCO_3^-, aq \quad (6)$$

and

$$HCO_3^-, aq \leftrightarrow H^+, aq + CO_3^{-2}, aq \quad (7)$$

As another example relevant to Enceladus, the pH regulates the availability of metals derived from minerals that have equilibrated with the solution. For the case of talc dissolution, we have

$$Mg_3Si_4O_{10}(OH)_2, talc + 6\ H^+, aq \leftrightarrow 3\ Mg^{+2}, aq + 4\ SiO_2, aq + 4\ H_2O, aq \quad (8)$$

By applying Le Chatelier's principle, it can be deduced that an increase in the activity of H^+ would shift the equilibrium to the right. Therefore, there should tend to be more Mg^{+2} in solution at lower pH.

There have been several attempts to estimate the pH of Enceladus' ocean. *Zolotov* (2007) performed calculations of chemical equilibrium between liquid water and rock of CI carbonaceous chondrite bulk composition. The latter may be representative of rocks in Enceladus' core if it has not undergone igneous differentiation by partial melting (*Médard and Kiefer,* 2017), which is unlikely for a body as small as Enceladus [vigorous hydrothermal circulation may also make it difficult to reach magmatic temperatures (*Travis and Schubert,* 2015; *Choblet et al.,* 2017)]. *Zolotov*'s (2007) calculations indicate that the rocks would be hydrated to primarily Mg-phyllosilicates during alteration, and a Na-Cl-CO_3-HCO_3 solution with a pH of ~10.9 (at 0°C for a water/rock mass ratio of 1) would be produced. The general character of the predicted solution is consistent with subsequent measurements by Cassini CDA (Table 1). Of course, we do not know whether water-rock equilibrium is reached, which is a crucial assumption.

Postberg et al. (2009) attempted to determine the pH of the ocean from CDA spectra of salt-rich ice grains from the plume. They fired a laser at laboratory solutions of known pH in experiments simulating impact ionization of these grains. The relative abundances of salt clusters [$Na(NaOH)_n^+$ and $Na(NaCl)_n^+$, where n signifies a positive integer] from the analog experiments were correlated to the pattern of clusters in the Enceladus spectra. The concept can be illustrated by considering the following reaction that occurs in the high-energy zone of a laser or ice grain impact

$$Na(NaCl)^+, g + OH^-, g \rightarrow Na(NaOH)^+, g + Cl^-, g \quad (9)$$

At higher pH, OH^- is more abundant, so a larger peak area ratio of $Na(NaOH)^+$ to $Na(NaCl)^+$ is observed. The pronounced peaks from $Na(NaOH)_{1-3}^+$ in the Enceladus spectra therefore imply a relatively basic pH. *Postberg et al.* (2009) inferred a pH of 8.5–9. A potential concern is the issue of whether laser ionization in the laboratory is a quantitative analog for impact ionization in the CDA instrument. The energy density of the laser can be tuned to match that of ice grain impacts, but it is presently unclear if there should be a 1:1 correspondence, or if the laser-calibrated pH could be offset from the pH of flash frozen ocean droplets that impact the instrument.

Marion et al. (2012) performed speciation calculations in the carbonate system (see equations (6) and (7)) to estimate the pH. In their model, they adopted input conditions of 0.2 molal chloride and an alkalinity ($\approx m_{HCO_3^-} + 2m_{CO_3^{-2}}$) of 0.05 eq kg^{-1} H_2O. These values are consistent with the CDA data (Table 1). Their interpretation of the INMS data (Table 2) was that the ocean is rich in dissolved gases. This led to the assumption that gas (clathrate) hydrates might be controlling the fugacity of CO_2. Hence, a high fugacity of CO_2 (0.349 bar) was adopted as an input parameter. Marion et al. computed the speciation of the system using the FREZCHEM code. The modeled pH ranged between ~5.7 and ~6.8. However, this estimate is probably too low because the adopted fugacity of CO_2 is too high (see below). The weakly acidic pH in their model is caused by the formation of carbonic acid at relatively high fugacities of CO_2. Rainwater on Earth represents a classic example of this phenomenon (*Drever,* 1997).

Hsu et al. (2015) suggested that the presence of nanosilica in Enceladus' ocean constrains the pH of the ocean. In their interpretation (see section 4.2.1), a cooled hydrothermal fluid that is supersaturated in amorphous silica can produce nanometer-sized particles only if the ocean has a moderately alkaline pH. Above a pH of ~10.5, amorphous silica becomes too soluble to maintain a stable colloidal phase, as implied by the reaction below

$$SiO_2, amorphous + OH^-, aq \rightarrow HSiO_3^-, aq \quad (10)$$

These considerations led *Hsu et al.* (2015) to propose a pH of ~8.5–10.5. A possible concern with this approach is that it depends on nanosilica being present in the ocean. *Hsu et al.* (2015) provided a number of supporting arguments that the nanosilica measured by CDA originates from E-ring ice grains, but nanosilica was not directly observed in either the plume or the E ring.

Glein et al. (2015) improved upon the carbonate speciation approach of *Marion et al.* (2012) in their effort to infer the pH. *Glein et al.* (2015) attempted to constrain the activity of CO_2 in the ocean not directly from the plume abundance of CO_2 (Table 2), but instead by trying to account for the evolution of the CO_2/H_2O ratio in the gas as it migrates from the ocean to space. A large amount of H_2O condenses during migration, as the tiger stripes (~200 K) are much colder than the ocean (~273 K). If it is assumed that CO_2 does not condense or condenses to a lesser extent owing to its greater volatility, then the CO_2/H_2O ratio in the plume should be greater than the ratio in the ocean source region. *Glein et al.* (2015) adopted this no condensation of CO_2 endmember, and used the sublimation curve of water ice to estimate the CO_2/H_2O ratio at the ocean. This allowed them to make estimates of the activity of CO_2, which were combined with the salt data (Table 1) to calculate the carbonate speciation of the ocean. The model returned a pH range of ~10.8–13.5. A caveat is that the assumption of no CO_2 condensation is at best an approximation, and could lead to a pH overestimate of perhaps ~1 unit. This is a concern because VIMS data demonstrate the condensation of CO_2 (*Brown et al.,* 2006), although the fraction that condenses is still being worked out (*Matson et al.,* 2018).

Table 4 summarizes the previously published estimates for the pH of the ocean of Enceladus. If the inconsistent values from *Marion et al.* (2012) are discarded, then we are left with a range from pH 8.5 to 13.5. This is the total uncertainty. The range is not small, but it is not a trivial problem to determine the pH of an ice-covered ocean using measurements made in space. Looking at the ranges in the remaining studies, we suggest a "best-fit" pH of ~9–11. This can be regarded as a compromise between the studies, and it is proposed as a working model for the Enceladus ocean.

3.2.3. Apparent oxidation state. In general, low-temperature natural waters do not have a unique oxidation state.

TABLE 4. Estimates for the pH of Enceladus' ocean.

Reference	pH Value
Zolotov (2007)	10.9
Postberg et al. (2009)	8.5–9
Marion et al. (2012)	5.7–6.8
Hsu et al. (2015)	8.5–10.5
Glein et al. (2015)	10.8–13.5
Recommendation (this work)	~9–11

Individual redox couples comprising reduced and oxidized forms of an element can be quantified by an oxidation state parameter (see below), but different redox couples will have different parameter values if the entire chemical system is not at redox equilibrium. The latter is almost always the case in low-temperature environments where the rates of electron transfer reactions are too sluggish to permit the attainment of equilibrium. Nevertheless, it is useful to define oxidation state parameters, as they give us a scale that can be used to make general comparisons between different geochemical environments in terms of whether reduction or oxidation is thermodynamically favored. This is essential for rationalizing the behavior of elements that can exist in multiple formal oxidation states (e.g., Fe, S, C, N).

Because of the great abundance of water in Enceladus' ocean, it makes sense to choose a redox parameter based on hydrogen or oxygen. Here, we choose the activity of H_2 (a_{H_2}) because H_2 was measured in Enceladus' plume, and a model has been developed to derive the H_2 molality (~activity) in the ocean from the plume measurement (*Waite et al.,* 2017). A higher H_2 activity means that there is a stronger thermodynamic drive for H_2 to reduce other species. The choice of H_2 activity to define a redox scale is simply one of convenience. Values of other commonly used redox parameters can be calculated using thermodynamic relations. For example, the O_2 fugacity (f_{O_2}) (*Frost,* 1991) is related to the H_2 activity via the disproportionation of water

$$2\ H_2O, aq \leftrightarrow 2\ H_2, aq + O_2, g \quad (11)$$

which has an equilibrium constant

$$K_{11} = \frac{a_{H_2}^2 f_{O_2}}{a_{H_2O}^2} = 10^{-98.3} \text{ at 0°C and 1 bar} \quad (12)$$

The minuscule value of this equilibrium constant implies that measurable amounts of H_2 and O_2 cannot coexist at equilibrium at 0°C. Therefore, if a measured H_2 or O_2 parameter is used to derive the other parameter, the derived parameter will be unphysically small, and is not "real" but an abstraction (*Anderson,* 2005).

Another widely used redox variable is the reduction potential (Eh) referenced to the standard hydrogen electrode (SHE). On this electrochemical scale, SHE (comprised of unit fugacity of H_2 gas and unit activity of H^+) is defined as the zero point. A half-cell reaction that allows one to relate the activity of H_2 to the corresponding Eh can be written as

$$2\ H^+, aq + 2\ e^-, aq \leftrightarrow H_2, aq \quad (13)$$

From the stoichiometry of this reaction, the Eh can be calculated using an appropriate form of the Nernst equation as shown below

$$Eh = E^\circ - \frac{2.3026RT}{nF}\left(\log a_{H_2} + 2pH\right) \quad (14)$$

where E° designates the standard reduction potential (–0.0983 V at 0°C and 1 bar), R the gas constant (8.3145 J mol^{-1} K^{-1}), T the absolute temperature, n the number of electrons transferred, and F Faraday's constant (96,485 C mol^{-1}).

It is not easy to determine the concentration of H_2 in the ocean of Enceladus from the mixing ratio of H_2 in the plume. One approach is to assume that the H_2/H_2O ratio is the same in the ocean as in the plume. However, this is problematic because water vapor condensation during transport should increase the gas-phase ratio of H_2/H_2O. Modeling can be performed to try to account for this effect, but that requires an assumption to be made with regard to the quench temperature for solid-vapor equilibrium of water in the tiger stripes (*Glein et al.,* 2015). A more robust approach is to find a different volatile ratio (i.e., one with a much less condensable reference species than H_2O) that would be minimally fractionated between the ocean and plume. An issue, however, is that deriving absolute concentrations in the ocean (e.g., the molality of H_2) from ratios of volatile gases in the plume requires a constraint on the absolute concentration of the reference species.

Waite et al. (2017) considered this state of affairs, and proposed an approach centered on CO_2 as the reference species. Carbon dioxide is much less susceptible to condensation than water because of its much greater volatility. Thus, it may be reasonable to assume that there is minimal condensation of CO_2 during transport, although some condensation must occur (*Brown et al.,* 2006). Another reason why CO_2 is a useful reference species is that its absolute concentration in the Enceladus ocean can be estimated using existing data from Enceladus. This can be done by evaluating the speciation of the carbonate system (see equations (6) and (7)) for specified values of $HCO_3^- + CO_3^{-2}$ concentration and pH. Constraints on these parameters can be found in Tables 1 and 4, respectively. To ascertain the range in H_2 activity (~molality) consistent with the present data, we consider high and low H_2 endmembers. For the high H_2 endmember, we determine the speciation for a solution containing 0.2 molal Cl^-, 0.1 molal $HCO_3^- + CO_3^{-2}$, and an aqueous H_2/CO_2 ratio of 4.7 (Table 2). The adopted composition for the low H_2 endmember is 0.05 molal Cl^-, 0.01 molal $HCO_3^- + CO_3^{-2}$, and $H_2/CO_2 = 0.5$ (Table 2). By solving the carbonate speciation problem [using The Geochemist's Workbench (*Bethke,* 2008)] over the recommended pH range of 9–11 at 0°C, the molality of CO_2 can be obtained. The activity of H_2 can then be estimated using the scaling relation

$$a_{H_2} \approx m_{H_2} = \left(\frac{H_2}{CO_2}\right)_{plume} \times m_{CO_2} \qquad (15)$$

Figure 4 shows derived values for the activity of H_2 in the ocean of Enceladus. Strictly speaking, these should be called apparent activities because they are model outputs based on plume data. The H_2 activity from this model is between ~2×10^{-8} and ~9×10^{-4}. The implied concentration range is ~20 nmolal to ~0.9 mmolal. The ranges in f_{O_2} and Eh are ~$10^{-92.2}$ to ~$10^{-83.0}$ bar [i.e., ~4.4 log f_{O_2} units less oxidized than the fayalite-magnetite-quartz (FMQ) buffer to ~4.8 log f_{O_2} units more oxidized than FMQ; see section 4.2.2], and –0.504 to –0.488 V, respectively. The trend of decreasing activity of H_2 with increasing pH (Fig. 4) reflects lower concentrations of aqueous CO_2 at higher pH. This relationship between pH and H_2 activity is a consequence of how the model is set up.

Three possible complications have been identified. First, freezing out ocean-derived CO_2 would decrease the apparent H_2 activity, while subliming CO_2 from the ice shell would increase the apparent H_2 activity. Second, the present lack of explanation for the observations of H_2 spikes by INMS (*Waite et al.,* 2017) could imply that they are generated by an instrumental effect. If an unknown instrumental effect can produce the rest of the H_2 signal (interpreted to be from native H_2) under different circumstances from the spikes, then the apparent H_2 activity would represent an upper limit [however, see *Waite et al.* (2017) for a detailed analysis of the instrument background at mass 2]. Third, the apparent H_2 activity is for the plume source region at the top of the ocean. Because H_2 is escaping from this region, the deeper ocean can be expected to have a higher activity of H_2. In this case, the derived values in Fig. 4 would be lower limits for the bulk ocean.

With constraints on the pH and activity of H_2 in Enceladus' ocean, we can place this environment into a broader context by comparing its conditions of pH-log a_{H_2} to the possible Earth analogs from section 3.2.1. To add the ana-

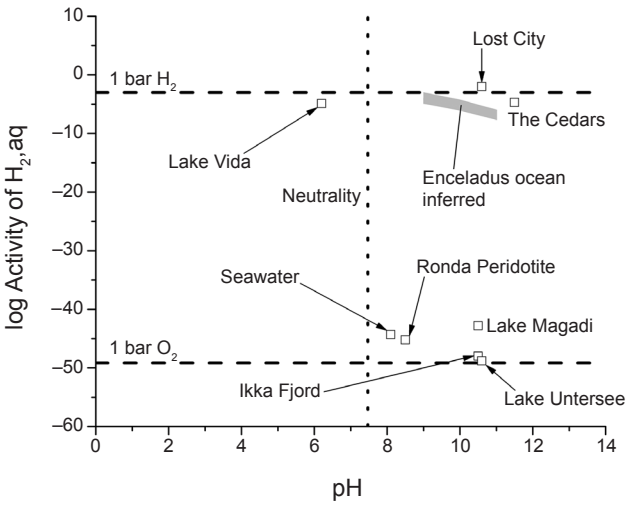

Fig. 4. Redox-pH conditions in Enceladus' ocean vs. potential terrestrial analogs (Table 3). The pH range for Enceladus is from Table 4, and the range in H_2 activity is determined by the range in H_2 mixing ratio in the plume according to the geochemical model described in section 3.2.3. Neutral pH at 0 °C is shown. The 1 bar H_2 line represents the solubility of 1 bar of H_2 from Henry's law, while the 1 bar O_2 line indicates the H_2 activity that would be in equilibrium with 1 bar of O_2.

logs to Fig. 4, we calculated the H_2 activity from measurements of the concentration of H_2 in fluids from Lost City (*Seyfried et al.,* 2015), the Cedars (*Morrill et al.,* 2013), and Lake Vida (*Murray et al.,* 2012). For the well-oxygenated other sites, we assumed that O_2 is the dominant controller of their redox chemistry, and we derived thermodynamic values of the H_2 activity consistent with equations (11) and (12) for the temperature of the site of interest (Table 3). In pH-log a_{H_2} space, Lost City and the Cedars appear to be most similar to the Enceladus ocean (Fig. 4). This suggests that reactions between water and ultramafic rocks could be influencing these properties of the ocean (*Glein et al.,* 2015) (see section 4.2.2). Lake Vida overlaps the Enceladus ocean in H_2 activity, but the former is significantly more acidic than the latter. Conversely, we find that the other sites are fairly consistent with the inferred pH of Enceladus' ocean, but the availability of abundant atmospheric O_2 on Earth makes them much more oxidized compared with the Enceladus ocean.

Overall, the composition of the Enceladus ocean resembles a hybrid of Ikka Fjord, seawater (see section 3.2.1), and Lost City/the Cedars. None of these sites capture all the essential features of Enceladus' ocean, but they each exhibit at least one key similarity to the inferred geochemical properties of the latter. Cassini discovered an ocean of sea salt and soda serpentinizing the underlying rocks.

4. HYDROTHERMAL GEOCHEMISTRY

4.1. Pressure and Temperature in the Rocky Core

We continue using the interior model of *McKinnon* (2015) to estimate pressures in the rocky core of Enceladus. Pressures inside the core can be calculated using the following formula (*Turcotte and Schubert,* 2002)

$$P = \frac{2}{3}\pi G\rho_c^2\left(R_c^2 - r^2\right) + \frac{2}{3}\pi G\rho_h^2\left(R_E^2 - R_c^2\right) + \frac{4}{3}\pi\rho_h G R_c^3\left(\rho_c - \rho_h\right)\left(R_c^{-1} - R_E^{-1}\right) \quad (16)$$

which is applicable to $0 \le r \le R_c$ (see section 3.1 for definitions of the parameters). Figure 5 shows the pressure profile below the ocean floor. According to this model, the pressure increases from an ocean floor value of ~74 bar to a maximum of ~377 bar at the center of the moon. The highest pressure in Enceladus is comparable to the average seafloor pressure on Earth (~400 bar).

It is more difficult to determine temperatures in the core (see the chapter by Castillo-Rogez et al. in this volume). Here, we attempt to set some conservative upper limits. In sections 4.2.1 and 4.2.2, we consider the temperature implications of models for hydrothermal SiO_2 and H_2, respectively. A first constraint is imposed by the liquid-vapor saturation curve of water. For a core with ~20–30% water-filled porosity (*Choblet et al.,* 2017; *Waite et al.,* 2017; *Vance et al.,* 2018), the boiling point represents the maximum temperature for pressures less than the critical pressure of H_2O (~221 bar). Figure 5 indicates that boiling would control the maximum temperature of hydrothermal fluids down to a depth of ~54 km beneath the ocean floor. Once a fluid is heated to the appropriate boiling temperature, any additional input of heat would not increase its temperature but would go into vaporizing water. At the ocean floor, the boiling temperature is ~290°C. This is the maximum temperature of aqueous fluids issuing into the ocean from hydrothermal vents. A large portion of the rocky core is subject to the boiling limit. Owing to the spherical geometry of the core, ~63% of its volume experiences pressures less than the critical pressure of H_2O. In this region (~74–221 bar; Fig. 5), the relationship between the pressure and maximum temperature (T_{max}) can be parameterized as (*Wagner and Pruß,* 2002)

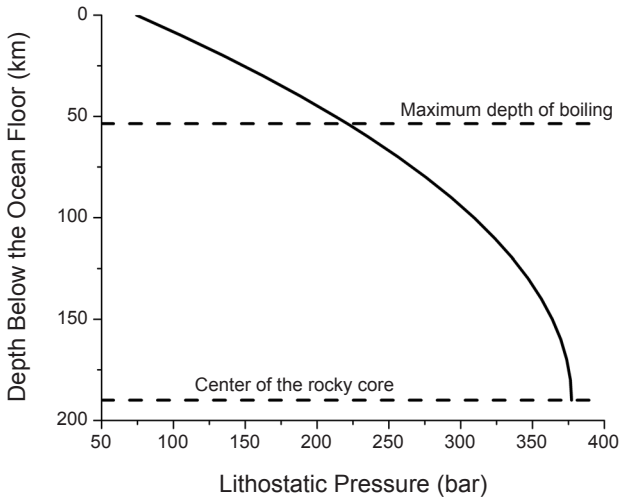

Fig. 5. Pressures in the rocky core of Enceladus based on the internal structure model of *McKinnon* (2015). The maximum depth of boiling is where the pressure equals the critical pressure of water (~221 bar).

$$\log P(\text{bar}) = 5.504 - \frac{2047}{T_{max}\,(\text{K})} \quad (17)$$

The boiling limit does not apply deep in the core (Fig. 5), so a different approach must be taken to constrain temperatures there. Because the density of Enceladus' core is rather low [~2450 kg m^{-3} (*Iess et al.,* 2014; *McKinnon,* 2015)], the core should be rich in hydrated silicates [although see *Vance et al.* (2018) for an anhydrous case]. This imposes a constraint on the temperature given that hydrated minerals undergo dehydration at sufficiently high temperatures. Dehydrating the rocks would make the core too dense. The argument can be quantified by performing a simple geochemical analysis. Here, we approximate the dehydration process by tracking the release of water from antigorite serpentine. Antigorite ($Mg_{48}Si_{34}O_{85}(OH)_{62}$) is the polymorph of serpentine that is most stable during metamorphism. Serpentine minerals are likely to dominate the budget of

mineral-bound water (i.e., OH) in the deep interior (*Zolotov,* 2007). To show that this is likely to be the case, one must go a step beyond the consensus of a heavily hydrated core, and consider specific hydroxylated silicates that could be present. *Waite et al.* (2017) developed a normative model for the mineralogy of possible rocks in the Mg-Si-Fe-S-O-H system on Enceladus. In their reduced hydrous rock, ~68% of the mineral-bound water is in Mg-serpentine, ~31% is in Fe(II)-serpentine, and ~1% is in talc/saponite. Their oxidized hydrous rock has ~69% of the mineral-bound water in Mg-serpentine and ~31% in talc/saponite. Thus, the mass balance supports a focus on the dehydration of antigorite to elucidate an approximate upper temperature limit.

The classic dehydration sequence of antigorite (*Tracy and Frost,* 1991) can be represented by the following reactions

$$\begin{aligned} &Mg_{48}Si_{34}O_{85}(OH)_{62}, \text{antigorite} \rightarrow \\ &4\ Mg_3Si_4O_{10}(OH)_2, \text{talc} + \\ &18\ Mg_2SiO_4, \text{forsterite} + 27\ H_2O, \text{aq} \end{aligned} \tag{18}$$

$$\begin{aligned} &4\ Mg_3Si_4O_{10}(OH)_2, \text{talc} + \\ &1.778\ Mg_2SiO_4, \text{forsterite} \rightarrow \\ &2.222\ Mg_7Si_8O_{22}(OH)_2, \text{anthophyllite} + \\ &1.778\ H_2O, \text{aq} \end{aligned} \tag{19}$$

and

$$\begin{aligned} &2.222\ Mg_7Si_8O_{22}(OH)_2, \text{anthophyllite} + \\ &2.222\ Mg_2SiO_4, \text{forsterite} \rightarrow \\ &20\ MgSiO_3, \text{enstatite} + 2.222\ H_2O, \text{aq} \end{aligned} \tag{20}$$

The curves in Fig. 6 show where these reactions would occur in pressure-temperature space. By summing equations (18) through (20), it can be found that the complete dehydration of 1 mole of antigorite releases 31 moles of water. Because equation (18) releases ~87% of the total H_2O, we deduce that this reaction effectively determines the content of bound water in rocks, and therefore their densities. To maintain a relatively low core density, temperatures in the core should be lower than the appropriate dehydration temperature of antigorite. The dehydration temperature increases with pressure (Fig. 6). For a maximum pressure of ~377 bar, the corresponding temperature is ~445°C. This can be regarded as an apparent (see below) upper limit for the present core.

Core temperatures could have been higher than ~445°C in the past if conduction was the dominant mode of heat transfer (*Schubert et al.,* 2007). In this case, the rocks would have needed to experience subsequent hydration to end up with a consistent density. Alternatively, advection of hydrothermal fluids could have always been the dominant heat transfer mechanism (*Choblet et al.,* 2017). The greater efficiency of advection provides a way of explaining the apparent persistence of hydrated minerals, by modulating increases in temperature. Nevertheless, it remains a possibility for a portion of the present core to be hotter than the antigorite limit if anhydrous rock exists at the center (*Malamud and Prialnik,* 2016).

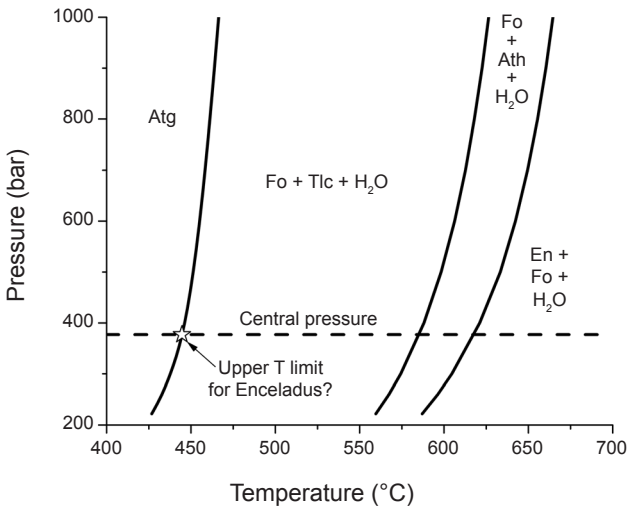

Fig. 6. Pseudosection phase diagram showing the stable phases for the initial composition of antigorite as a function of temperature and pressure. Central pressure refers to the pressure at the center of Enceladus' rocky core. A core rich in hydrated rock may not exceed the dehydration temperature of antigorite (see section 4.1). Mineral abbreviations: Atg, antigorite; Ath, anthophyllite; En, enstatite; Fo, forsterite; Tlc, talc. Thermodynamic data used to construct this diagram were taken from the SUPCRT database (*Helgeson et al.,* 1978).

4.2. Proposed Hydrothermal Species

4.2.1. SiO_2. *Hsu et al.* (2015) identified silica as the only significant constituent in saturnian stream particles, and inferred that these particles are being erupted inside ice grains from the Enceladus plume. They proposed that silica nanoparticles form at the ocean floor of Enceladus, where Si-enriched hydrothermal fluids mix with the cold ocean. The solubility of amorphous silica increases with temperature, so cooling promotes supersaturation, which is necessary to form colloidal silica.

Would enceladean hydrothermal fluids contain a sufficient concentration of dissolved silicon? Hydrothermal experiments with a mixture of olivine and orthopyroxene were performed to address this question (*Sekine et al.,* 2015). These minerals are thought to have been the most abundant silicates in accreted rocks. However, the experiments did not include Na- or Ca-rich silicates, which can have a strong influence on the speciation of fluids (*Zolotov and Postberg,* 2014). *Sekine et al.* (2015) found that the Si concentration in their experimental hydrothermal fluid was similar to that predicted for a fluid in equilibrium with serpentine and talc. Indeed, X-ray diffraction analysis revealed that serpentine and saponite (a trioctahedral phyllosilicate compositionally

similar to the Al-free endmember talc) are the major alteration minerals. To constrain the formation temperature of the silica nanoparticles, *Sekine et al.* (2015) performed speciation calculations under the assumption that the activity of SiO_2 in hydrothermal fluids on Enceladus would be similar to that determined by a serpentine-talc buffer, such as

$$0.5\ Mg_3Si_4O_{10}(OH)_2, \text{talc} + 0.5\ H_2O, \text{aq} \leftrightarrow 0.5\ Mg_3Si_2O_5(OH)_4, \text{chrysotile} + SiO_2, \text{aq} \quad (21)$$

In alkaline systems, $HSiO_3^-$ and $NaHSiO_3$ can be more abundant than aqueous SiO_2. There is a pH effect as indicated by the following equilibria

$$SiO_2, \text{aq} + H_2O, \text{aq} \leftrightarrow H^+, \text{aq} + HSiO_3^-, \text{aq} \quad (22)$$

and

$$Na^+, \text{aq} + HSiO_3^-, \text{aq} \leftrightarrow NaHSiO_3, \text{aq} \quad (23)$$

which imply that the concentrations of both $HSiO_3^-$ and $NaHSiO_3$ should increase at higher pH. The minimum temperature required to precipitate amorphous silica as a result of cooling depends on the pH of the hydrothermal fluid and that of ocean water. *Sekine et al.* (2015) used their speciation results to map out these relationships. They suggested that the minimum temperature would be ~150°–200°C if the compositions of the hydrothermal fluid and ocean water are controlled by the same water-rock equilibria. If the two fluids are treated as pH-decoupled systems, then the model of *Sekine et al.* (2015) indicates that the minimum temperature could be decreased to a value as low as ~50°C if the hydrothermal fluid pH is ~2 units higher than the ocean pH.

To test if rocks containing serpentine and talc can generate sufficiently Si-rich fluids that would precipitate amorphous silica upon cooling, the pH of the fluids must be modeled self-consistently. One way to do this is to assume that the rocks would also contain calcite ($CaCO_3$) and tremolite ($Ca_2Mg_5Si_8O_{22}(OH)_2$). Downwelling of ocean water into the rocky core would bring carbonate species (Table 1) in contact with rocks deeper in the core, facilitating the formation of calcite. For a deep rock endmember (see section 4.2.2), we envision that some of the calcium is still in silicate minerals, thus tremolite is chosen as a model mineral to simulate the pH effect. The assemblage chrysotile-talc-calcite-tremolite sets the activity of CO_2 according to

$$3\ Ca_2Mg_5Si_8O_{22}(OH)_2, \text{tremolite} + 2\ Mg_3Si_2O_5(OH)_4, \text{chrysotile} + 6\ CO_2, \text{aq} \leftrightarrow 6\ CaCO_3, \text{calcite} + 7\ Mg_3Si_4O_{10}(OH)_2, \text{talc} \quad (24)$$

To complete the model, it is assumed that the hydrothermal fluid inherits the chlorinity and carbonate alkalinity of the downwelling ocean water. We adopt a nominal chlorinity of 100 mmolal and a total carbonate concentration of 30 mmolal (see section 3.2.1), which translates to a carbonate alkalinity of 31 and 56 meq kg^{-1} H_2O for pH 9 and 11, respectively. With constraints on the activity of CO_2 and carbonate alkalinity, the pH can be evaluated from the speciation of the hydrothermal fluid. Here, the speciation is computed using the GEOCHEQ code (*Zolotov,* 2012).

Hydrothermal fluids with compositions described by this geochemical model would be relatively poor in dissolved silicon (Fig. 7). The chrysotile-talc buffer (see equation (21)) does not yield high activities of SiO_2. The pH of the hydrothermal fluid is predicted to decrease with temperature from ~10.5 (~4 units above neutral) at 50°C to ~8 (~2 units above neutral) at 350°C. There is more silica in the modeled fluid at the higher alkalinity because the pH is ~0.1–0.2 units higher. The modeled fluid is generally deficient in dissolved silicon for the case of a pH 9 ocean, and the model is definitely incapable of achieving amorphous silica saturation for the case

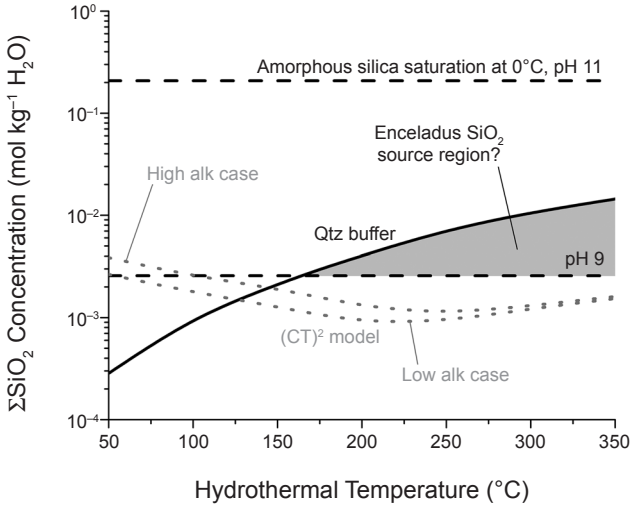

Fig. 7. Total concentration of silica species ($\Sigma SiO_2 \approx SiO_2$,aq + $HSiO_3^-$ + $NaHSiO_3$,aq) in hydrothermal fluids on Enceladus from equilibrium with quartz (Qtz; solid curve), or with chrysotile-talc-calcite-tremolite [$(CT)^2$; dotted gray curves]. The dashed horizontal lines show the saturation state of amorphous silica for the indicated ocean pH at a constant temperature of 0°C. In this representation (see Fig. 9), hydrothermal fluids leach Si from silicates in the core, and then cooling of the fluids in the ocean causes amorphous silica to precipitate if the hydrothermal equilibrium curve lies above the appropriate saturation line. The low and high alk curves for the $(CT)^2$ model should be compared to the values for pH 9 or 11, respectively, while the quartz curve can be compared to either of the saturation values (see section 4.2.1). The gray region provides a lower limit on temperatures of amorphous silica-forming hydrothermal fluids from the rocky core. Amorphous silica rather than quartz is the relevant precipitating phase of SiO_2 for fluids that undergo rapid cooling (as in siliceous sinter-depositing hot springs at Yellowstone National Park), because the disordered structure is kinetically/mechanistically easier to form.

of a pH 11 ocean (Fig. 7). The latter observation supports the conclusion of *Hsu et al.* (2015) that the pH of the ocean should not be too high to allow nanophase silica to form.

The $(CT)^2$ model can provide enough silica if the ocean pH is lower than ~9 and if the hydrothermal temperature is below ~50°C; the enhancement in dissolved silicon follows from the high pH of such low-temperature hydrothermal fluids. This underscores the possible role of a gradient between high pH fluids in the core and lower pH ocean water driving the formation of amorphous silica (*Sekine et al.,* 2015). Similarly, NaOH-rich core fluids if present would dramatically increase the solubility of silicates, especially at low temperatures (*Zolotov,* 2012). At temperatures above ~50°C, the concentration of dissolved silicon predicted by the pH 9 ocean model is generally a factor of ~2–3 lower than required (Fig. 7). We interpret this to mean that achieving consistency may not be impossible, but hydrothermal alteration of chondritic rock inside Enceladus' core would not provide a robust mechanism for making amorphous silica. This conclusion is further supported by the more detailed geochemical modeling of *Zolotov and Postberg* (2014), who showed that fluids in equilibrium with altered chondritic rock could be even more deficient in dissolved silicon (by up to about 1 order of magnitude).

We wish to clarify that it is a misconception to assume that fluids compositionally similar to those at Lost City would precipitate amorphous silica at Enceladus. There is not enough dissolved silicon in Lost City fluids, by ~1–2 orders of magnitude (*Seyfried et al.,* 2015). Amorphous silica at Enceladus can be used to argue for the existence of hydrothermal systems (see below), but not systems that are geochemically analogous to Lost City (i.e., serpentinization systems).

There is motivation to identify more robust mechanisms for producing amorphous silica inside Enceladus. We introduce a possibility that involves hydrothermal processing of quartz-bearing rocks. This is usually how amorphous silica is produced by hydrothermal processes on Earth (*Fournier and Rowe,* 1966; *Von Damm et al.,* 1985). Quartz-bearing rocks could be present as a weathering crust on the core of Enceladus. Such rocks can be formed via the process of carbonation (*Klein and Garrido,* 2011), where carbonate derived from CO_2 serves as a sink of divalent cations such as magnesium, leaving behind Si-enriched phases. As an example of such chemistry, *Streit et al.* (2012) reported a remarkable occurrence of quartz that apparently formed by carbonation of serpentinized peridotite at ambient temperatures on Earth. Carbonation of rocks on Enceladus would be promoted by the accretion of a large amount of CO_2, as observed at numerous comets (*Ootsubo et al.,* 2012). The relatively high abundance of (bi)carbonate salts in many plume particles (Table 1) provides evidence for the reaction of CO_2 with rocks. Enceladus' ocean floor has presumably experienced the most intense chemical weathering, because that is where the volatiles-to-rock ratio should be largest.

The solubility curve of quartz in Fig. 7 corresponds to the following equilibrium

$$SiO_2, \text{quartz} \leftrightarrow SiO_2, \text{aq} \quad (25)$$

The curve does not account for variable pH, but GEOCHEQ calculations showed that neutral SiO_2 would be the dominant Si species (>80% of dissolved Si) in heated ocean water that had equilibrated with quartz, magnesite ($MgCO_3$), and talc (a possible carbonation assemblage in the weathering crust). Hydrothermal fluids in equilibrium with quartz would be rich in dissolved silicon (Fig. 7). Quartz-buffered fluids at temperatures above ~165°C would contain sufficient silica to precipitate amorphous silica into a pH 9 ocean. This is a lower limit on temperatures in the source region of the silica nanoparticles. The pH of the ocean would also be constrained; if we assume a hydrothermal temperature of ~350°C, then amorphous silica precipitation from a quartz-buffered fluid is possible only if the ocean has a pH lower than ~10. The range in the concentration of silica from the quartz model (~3–15 mmolal from ~165° to 350°C; Fig. 7) is consistent with the observationally based estimate (~2.5–65 mmolal) of *Hsu et al.* (2015).

4.2.2. H_2. The INMS instrument detected H_2 in the plume (Table 2), and it was concluded that the H_2 is native to Enceladus (*Waite et al.,* 2017). In addition to water-rock processes such as serpentinization (*Vance et al.,* 2007), there are several other candidate sources of H_2 that must be considered. One possibility is that the H_2 is primordial, and was acquired by gravitational capture from the saturnian subnebula, or by trapping in cold amorphous ices. However, these sources can be ruled out based on the lack of detection of ^4He ($^4He/H_2O < 6 \times 10^{-5}$) and ^{36}Ar ($^{36}Ar/H_2O < 4 \times 10^{-6}$), respectively, in the plume gas (*Waite et al.,* 2017). Another possible source of H_2 is thermal cracking of NH_3 to N_2 and H_2 (*Matson et al.,* 2007). But, this mechanism is unattractive owing to the non-detection of N_2 ($N_2/H_2O < 5 \times 10^{-4}$). Alternatively, the H_2 could be radiolytic, and might have been produced from H_2O by radiation chemistry at the surface or in the interior (*Bouquet et al.,* 2017). Both of these processes should be ongoing, but kinetic calculations suggest that neither of them can make enough H_2 to account for the observations (*Waite et al.,* 2017). Conversely, mass balance calculations indicate that huge amounts of H_2 can be generated by reactions between water and reduced minerals, or by pyrolysis of organic matter (*Waite et al.,* 2017). The H_2-generating potential of both of these sources is sufficient to sustain the present level of outgassing over the history of the solar system. *Waite et al.* (2017) therefore suggested that the H_2 is likely produced by hydrothermal processing of rocks containing both ferrous iron-bearing silicates and organic materials. They further argued that this process is occurring today, as the H_2/CH_4 ratio may be much lower than the observed value (~1–14) if the H_2 had been stored in impermeable rocks and released recently.

The following questions remain: (1) How can mineral vs. organic sources of H_2 be discriminated? (2) Would the formation of carbonate minerals affect the yield of H_2? (3) How does the H_2 abundance in the plume relate to hydrothermal conditions in the rocky core? We develop a model that can

be used to predict the mixing ratio of H_2 in the plume gas based on geochemical and geophysical properties of a globally averaged hydrothermal system. The rate at which H_2 is delivered via hydrothermal vents to Enceladus' ocean (δ_{H_2}) is given by the product of the molal concentration of H_2 in hydrothermal fluids (m_{H_2}) times the mass flow rate of hydrothermal fluids (Q_{H_2O})

$$\delta_{H_2} = m_{H_2} Q_{H_2O} \tag{26}$$

We consider three simplified source materials for making H_2: (1) rocks buried deep in the core ("deep rocks"), (2) rocks near the ocean floor ("shallow rocks"), and (3) organic materials ("organics"). For deep rocks, we assume that their equilibrium oxidation state is similar to that of rocks on Jupiter's moon Io. Io's rocks might be representative of relatively reduced silicate assemblages in the outer solar system. We adopt an oxidation state that is 2 log f_{O_2} units below the fayalite-magnetite-quartz buffer (*Zolotov and Fegley,* 2000). This is equivalent (see equation (12)) to an H_2 activity that is 1 log a_{H_2} unit above FMQ. The FMQ buffer can be represented by

$$\begin{aligned} &1.5\ Fe_2SiO_4, \text{fayalite} + H_2O, \text{aq} \leftrightarrow \\ &Fe_3O_4, \text{magnetite} + 1.5\ SiO_2, \text{quartz} + H_2, \text{aq} \end{aligned} \tag{27}$$

Using thermodynamic data from *Helgeson et al.* (1978) and *Shock et al.* (1989) and assuming that aqueous H_2 behaves ideally, we derive the following relationship for this model of deep rocks on Enceladus

$$\begin{aligned} &\log m_{H_2}\left(\text{deep rocks}\right) = \\ &-37.87 + \frac{644.4}{T(K)} + 5.56 \times \ln\left(T(K)\right) \end{aligned} \tag{28}$$

which is applicable to temperatures from 273 to 623 K (0°–350°C).

For shallow rocks in the core, we consider the possibility of an extensively carbonated ocean floor (see section 4.2.1), and therefore assume that Fe-bearing carbonate (e.g., siderite ($FeCO_3$)) is the key mineral carrier of iron (*Ueda et al.,* 2016). The oxidation of Fe(II) in siderite to Fe(III) in magnetite can generate H_2 if this process is coupled to the reduction of H_2O, which could occur as follows

$$\begin{aligned} &3\ FeCO_3, \text{siderite} + Mg_3Si_4O_{10}\left(OH\right)_2, \text{talc} \leftrightarrow \\ &Fe_3O_4, \text{magnetite} + 3\ MgCO_3, \text{magnesite} + \\ &4\ SiO_2, \text{quartz} + H_2, \text{aq} \end{aligned} \tag{29}$$

The equilibrium concentration of H_2 for this reaction is given by (*Helgeson et al.,* 1978; *Shock et al.,* 1989)

$$\begin{aligned} &\log m_{H_2}\left(\text{shallow rocks}\right) = \\ &-54.48 - \frac{364.3}{T(K)} + 8.02 \times \ln\left(T(K)\right) \end{aligned} \tag{30}$$

from 273 to 623 K (0°–350°C).

The concentration of H_2 in hydrothermal fluids cooking organic matter in Enceladus' core can be represented by

$$m_{H_2}\left(\text{organics}\right) = \frac{\left(O/R\right)}{\left(W/R\right)} Y_{H_2} \tag{31}$$

where O/R and W/R correspond to the organic/rock and water/rock mass ratios, respectively; and Y_{H_2} designates the yield of H_2 in mol per kilogram of organic matter. Here, we adopt W/R = 1 for hydrothermally active regions in Enceladus' core, and O/R = 0.4, a value intermediate between CI chondrites (*Alexander et al.,* 2007) and dust particles from Comet 67P (*Bardyn et al.,* 2017). The parameterization of *Waite et al.* (2017), based on the Murchison meteorite (*Okumura and Mimura,* 2011), is used to estimate the pyrolytic yield of H_2. Equation (31) then becomes

$$\log m_{H_2}\left(\text{organics}\right) = 3.55 - \frac{4023}{T(K)} \tag{32}$$

The H_2 yield was fit to experimental data from 350° to 800°C, but this equation can be extrapolated to lower temperatures, as the functional form is consistent with thermodynamic (van't Hoff equation) or kinetic (Arrhenius equation) control of the H_2 yield in the experiments of *Okumura and Mimura* (2011).

The mass flow rate of hydrothermal fluids (see equation (26)) can be estimated using an approach similar to that of *Lowell and DuBose* (2005). The basis of the approach is energy conservation for heat that is transported by hydrothermal fluids into the Enceladus ocean. We found that heat capacities (C_p) for liquid water at 300 bar can be represented by (*Wagner and Pruß,* 2002)

$$C_p = \alpha + \beta \times T^9 \tag{33}$$

with α = 4130 J kg^{-1} K^{-1} and $\beta = 1.53 \times 10^{-22}$ J kg^{-1} K^{-10} for 273–623 K (0°–350°C). For this functional form of the heat capacity, the rate of heat transfer (H) is related to the mass flow rate by

$$H = Q_{H_2O}\left[\alpha\left(T_{hydro} - T_{ocean}\right) + 0.1 \times \beta\left(T_{hydro}^{10} - T_{ocean}^{10}\right)\right] \tag{34}$$

where T_{hydro} refers to the hydrothermal fluid temperature, and T_{ocean} the temperature of Enceladus' ocean. We can obtain Q_{H_2O} as a function of T_{hydro} by specifying a value for H. Below, we consider a range of 1–10 GW based on *Choblet et al.*'s (2017) model of tidal dissipation and fluid flow in Enceladus' core.

If the concentration of H_2 in Enceladus' ocean has reached a steady state between hydrothermal input and output from the plume, then the latter rate is also given by equation (26). The molar ratio of H_2/H_2O that would be expected in the plume gas can be computed from the rate of H_2 output from the preceding hydrothermal model, and

the emission rate of water vapor from the plume. A value of 200 kg s^{-1} (11,000 mol s^{-1}) is adopted for the latter quantity (*Hansen et al.,* 2011).

Figure 8 compares H_2/H_2O ratios predicted to be in the plume gas from the three sources vs. the observed range. The models of organic pyrolysis, and hydrothermal processing of shallow rocks, do not provide enough H_2, as their fluids are too dilute in H_2 (<1 mmolal). Making these models consistent with the H_2 observations apparently requires over ~50 GW of heat to be transferred by advection of these fluids. In contrast, the deep rock model can explain the measurement of H_2 if the hydrothermal temperature is higher than ~170°C (Fig. 8). Higher temperatures would be needed if H is lower, and vice versa. However, a value of H less than ~1 GW may not yield sufficient H_2. Therefore, the observations of H_2 in the plume appear to provide support to the idea that tidal heating is taking place in Enceladus' core, and a large amount of heat is being transferred by fluid circulation (*Choblet et al.,* 2017). It should be noted, however, that hydrothermal activity would not have to be as vigorous if the rock is more reduced than the Io model. The H_2 measurement also imposes a limit on the oxidation state of deep rocks. They should not be more oxidized than the FMQ buffer; otherwise, the fluid would not be sufficiently rich in H_2 (>10 mmolal) to account for the measurement. These calculations suggest that H_2 in the plume (*Waite et al.,* 2017) can be taken as evidence for chemical interactions between hot fluids and reduced minerals relatively deep in the core of Enceladus.

4.2.3. Self-consistency? There is a potential inconsistency between the explanations for hydrothermal SiO_2 and H_2. The quartz buffer in section 4.2.1 is part of the shallow rock model in section 4.2.2. Hydrothermal processing of this rock can be the source of the silica (Fig. 7) detected by CDA (*Hsu et al.,* 2015), but not the molecular hydrogen (Fig. 8) detected by INMS (*Waite et al.,* 2017). On the other hand, the $(CT)^2$ model (section 4.2.1) is an unfavorable source of SiO_2 (Fig. 7), but the corresponding deep rock model in section 4.2.2 is the favored source of H_2 (Fig. 8). Theory shows that a low SiO_2 activity is one of the chief factors that enables a high H_2 activity to be created during serpentinization (*Frost and Beard,* 2007). This general expectation is borne out by an inverse correlation between the concentrations of H_2 and Si in ultramafic-hosted hydrothermal fluids (*Seyfried et al.,* 2011). In our modeling, one rock needs to be invoked to explain the SiO_2 observation, while the other rock is required to explain the H_2 observation; neither rock can explain both observations. What does this mean?

There could be multiple source rocks of hydrothermally derived species. Figure 9 shows a scenario illustrating how this might occur in a self-consistent manner. Hydrothermal fluids may react with reduced rocks if the fluids descend sufficiently. This would lead to the production of H_2, which dissolves in the fluids under pressure. As they rise back to the ocean floor, the fluids may intersect and react with quartz-bearing rocks, which would enrich the fluids in dissolved silicon. The H_2 produced at depth may survive passage through the shallow rock layer if iron there is sequestered in carbonate minerals (see section 4.2.2). Finally, fluids rich in both H_2 and SiO_2 may vent into the ocean of Enceladus, which could explain the observations by Cassini. The complexity of this hypothesis may accord with what might be expected of a geologically active world. As an example of this type of multi-rock model, *Seyfried et al.* (2015) found that Lost City fluids contain more silica than the very low concentrations expected for peridotite alteration. These researchers therefore suggested that Lost City

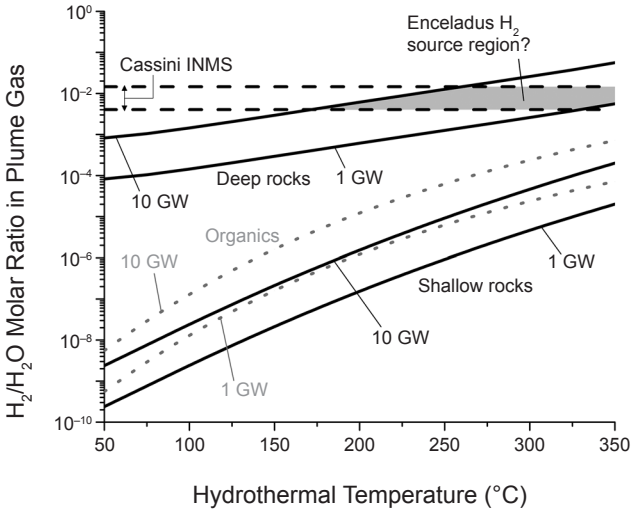

Fig. 8. Predicted abundance of H_2 in the Enceladus plume from hydrothermal models for H_2 production (see section 4.2.2) from deep rocks (top set of solid curves), organics (dotted gray curves), and shallow rocks (bottom set of solid curves). The dashed lines indicate the observational range for H_2 (Table 2). The gray region provides a lower limit on temperatures of H_2-producing hydrothermal systems in the rocky core.

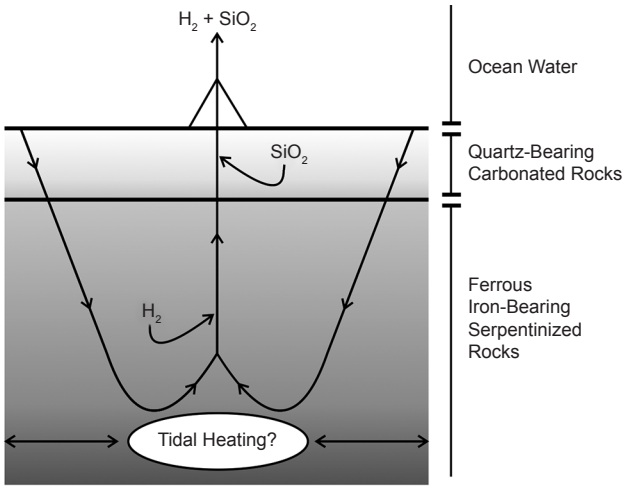

Fig. 9. Conceptual model for the formation of high H_2-high SiO_2 hydrothermal fluids by convective fluid flow through two different types of rocks under the ocean floor of Enceladus.

peridotite was intruded by more silicic rocks (e.g., gabbro), as often observed in peridotites dredged from the seafloor.

5. SOME GEOCHEMICAL QUESTIONS FOR THE FUTURE

Cassini gave humanity our first "taste" of enceladean geochemistry. There is still much to learn. In our view, finding ways to address the following questions should be considered a high priority for future studies.

How accurately can the composition of the ocean be inferred from that of the plume? Approaches have been developed to estimate the concentrations of ions (*Postberg et al.,* 2009) and gases (*Waite et al.,* 2017) in Enceladus' ocean using mass spectrometry data from salt-rich ice grains and the plume gas, respectively. However, the exclusion of a portion of salts during the freezing of ocean water, or vapor condensation onto grains in the tiger stripes, will inevitably fractionate them with respect to the composition of the ocean. Likewise, the gas composition could be fractionated between the ocean and plume by adsorption on ice, or clathrate formation (*Bouquet et al.,* 2015) or decomposition (*Kieffer et al.,* 2006; *Fortes,* 2007). We do not know at present how large these effects might be, nor their dependence on the physical properties of individual species. This necessitates a deeper understanding of how dynamical processes leading to plume formation influence the composition of the plume (see the chapter by Goldstein et al. in this volume). One path forward is to build a plume in the lab to investigate the plume's dynamical effects.

What are the concentrations of minor species in the ocean? A first step is to set upper limits on currently undetected ions using plume or E-ring data from Cassini CDA. Such constraints would be geochemically useful. Important species that have yet to be quantified include Ca^{+2}, Mg^{+2}, and SO_4^{-2}. Both Ca^{+2} and Mg^{+2} would provide information on mineral controls (e.g., carbonates) of ocean composition, while SO_4^{-2} could serve as a tracer of oxidant production or delivery to the ocean (*Ray et al.,* 2017). A direct measurement of the concentration of silica in ice grains from the plume (*Hsu et al.,* 2015) should be a high priority. This could be used to evaluate the saturation indices of different silicate minerals in contact with Enceladus' ocean. A wet chemistry laboratory on a south polar lander could allow silica and other aqueous species to be measured.

What is the detailed redox chemistry of the ocean? Enceladus appears to have a relatively reduced ocean as H_2, NH_3, and CH_4 are abundant in the plume gas (Table 2). However, CO_2 is also present and the CO_2-CH_4 couple is apparently out of equilibrium with the H_2O-H_2 couple (*Waite et al.,* 2017). Because there is geophysical activity to drive fluid mixing, other redox couples can be expected to be maintained in disequilibrium states in a cold ocean. This is vital for establishing the availability of chemical energy sources that could support life. How can we address this fundamental question? First, we should corroborate that the ocean is indeed reduced. CH_4, NH_3, and H_2 could be remeasured at slower flyby speeds (<5 km s^{-1}) to verify that they are not produced from ice-grain impacts on spacecraft instrumentation (*Waite et al.,* 2009). A complementary suite of reduced species are recommended to be measured in salt-rich plume particles, which could include Fe^{+2} and formate ($HCOO^-$). Second, our knowledge of redox disequilibria in the Enceladus ocean would be revolutionized if a comprehensive survey of gaseous and ionic H, O, C, N, and S species in the plume is performed.

Are there gradients in the composition of the ocean or the rocky core? Degassing could make the top of the ocean compositionally distinct (e.g., higher pH, lower H_2) from lower layers. Heterogeneous heating could create complex patterns of fluid flow that result in a redistribution of chemical elements. The development of coupled geophysical-geochemical models of reactive transport inside Enceladus would help the scientific community to better understand the consequences of such processes. For example, a rigorous assessment of the hypothesis outlined in section 4.2.3 requires quantitative results for the compositional evolution of both fluids and rocks as fluid parcels interact with rocks along reaction paths underneath the ocean floor (*McCollom and Shock,* 1998). Detailed geophysical modeling of both hydrothermal (*Choblet et al.,* 2017) and ocean circulation is needed to constrain rates of mixing and thus residence times of fluids in different geochemical environments on Enceladus. Modeling studies of these types offer opportunities for testing, refining, and differentiating between competing hypotheses. They therefore represent an important bridge between Cassini and plans to design future missions to Enceladus (see the chapter by Lunine et al. in this volume). A notable example of a useful probe of material interfaces in the subsurface and their associated compositional gradients would be a landed seismometer (*Stähler et al.,* 2018).

What geochemical evolutionary pathway did Enceladus take? The bulk composition of rocks accreted by Enceladus is commonly assumed to have been similar to that of CI chondrites, and Enceladus might have accreted volatiles in proportions similar to those in some comets (see the chapter by McKinnon et al. in this volume). It is still an open question as to how an initial mixture of chondritic rock and cometary ices (*Zolotov,* 2012) relates to the current composition of Enceladus as summarized in this chapter. To obtain insights into the formation conditions and accreted composition of Enceladus, additional cosmochemical data from Enceladus are needed such as a more precise value for the D/H ratio in H_2O (*Waite et al.,* 2009), a value for the $^{15}N/^{14}N$ ratio in NH_3, the abundances of primordial noble gases, and triple oxygen-isotope ($^{18}O/^{16}O$, $^{17}O/^{16}O$) measurements in samples of water ice from the plume. Considerable progress toward understanding the history of Enceladus could be made by elucidating the specific reactions and processes that would link plausible models of Enceladus' initial composition to its present geochemical state. Geochemical mass transfer modeling should be performed to learn what can happen if initial mixtures of frozen volatiles and ultramafic rocks were subjected to heating, water-rock separation, fluid circulation, and outgassing from the plume. Can the

ocean floor really become heavily carbonated? How would Fe(II) and Fe(III) partition among minerals, and what are the implications for H_2 production during serpentinization?

How representative are thermodynamic models of water-rock interaction for conditions relevant to Enceladus? We are advocating for experimental work that could be done to assess if chemical equilibrium is an appropriate assumption for aqueous solutions and altered rocks inside Enceladus. *Neveu et al.* (2017) took a step in this direction by comparing chemical equilibrium predictions to literature results from hydrothermal experiments with olivine or basalt. They found general agreement in the solid and fluid compositions, but the error in the predicted pH for the basalt experiments was ~1 unit. This may reflect inaccuracies in the thermodynamic properties of clay minerals in existing databases. Further comparisons between models and experiments may suggest strategies for improving the models. As a next step, it would help if such comparisons were made for volatile-rich chondritic compositions (e.g., a melted lab-made comet), particularly at temperatures closer to 0°C.

What new observations can be made to test for hydrothermal activity? The observations of SiO_2 and H_2 made by the Cassini spacecraft represent the first recognized indications of hydrothermal geochemistry (*Hsu et al.,* 2015; *Waite et al.,* 2017). Additional complementary data are desired, and their promise beckons us to go back to Enceladus. We should search for other chemical species (e.g., H_2S, CO) that may exhibit anomalous enrichments in the plume, consistent with the presence of fluids that are hot and reduced. A defining feature of hydrothermal activity is an elevated temperature relative to the ambient environment. Specific constraints on temperatures of core fluids on Enceladus can be obtained using tools of geothermometry, including isotopic ratios in simple volatiles [e.g., H_2-H_2O (*Horibe and Craig,* 1995)], ratios of certain organic compounds (e.g., ethylene/ethane; *Seewald,* 1994), and "clumping" of rare isotopes [e.g., $^{13}CH_3D$ (*Stolper et al.,* 2014)]. Measurements of radiogenic (mainly rock-derived) noble gases (primarily ^{40}Ar and ^{4}He) are also recommended as indicators of the extent and vigor of hydrothermal transport from the core to the hydrosphere.

What is the organic geochemistry of Enceladus? Data from both INMS and CDA show that the plume contains organic materials (*Waite et al.,* 2009; *Postberg et al.,* 2018). This is consistent with the association of an organic spectral signature with the tiger stripes (*Brown et al.,* 2006). The organic molecules detected by CDA are massive, rich in unsaturated carbon atoms in the form of unfused benzene rings, contain O- or N-bearing groups, and are probably phase-separated as solids from ocean water (*Postberg et al.,* 2018). At high spacecraft flyby velocities (>14 km s^{-1}), these molecules at least partially decompose to the smaller unsaturated molecules observed by INMS (*Waite et al.,* 2009). What is the origin of Enceladus' organic matter? Possibilities include accreted materials analogous to insoluble organic matter in chondrites (*Alexander et al.,* 2007); hydrothermal synthesis from small molecule precursors such as CO_2, HCN, formaldehyde, or methanol; and biological carbon fixation (see the chapter by McKay et al. in this volume). We emphasize that composition is the key to origin. Clues are needed in the form of measurements of the elemental and isotopic compositions of the particulate organic matter, as well as its functional group chemistry and structure. Pyrolysis-gas chromatography-mass spectrometry of south polar surface samples would be useful in this respect. We are also in need of detailed compositional characterizations of hydrocarbon gases (*Waite et al.,* 2009), and forms of dissolved organic carbon (e.g., fatty and amino acids) that may be present in the plume. Only with a more complete dataset will we be able to arrive at an integrated understanding of the geochemistry of Enceladus.

Acknowledgments. C.R.G. is grateful to J. Baross, M. Cable, J. Castillo-Rogez, F. Klein, J. Lunine, W. McKinnon, K. Miller, C. Porco, K. Rogers, E. Shock, N. Sleep, and H. Waite for numerous discussions on the geochemistry of Enceladus. C.R.G. wishes to express his appreciation to M. Zolotov for giving him a copy of the GEOCHEQ code. C.R.G. would also like to give thanks to the organizers of the 2nd Annual Ocean Worlds meeting at Woods Hole, where some of the new ideas in this chapter were first presented. J. Dao and R. Menchaca deserve recognition for their superb assistance in the preparation of Figs. 1 and 9. The work of C.R.G. was supported by the Cassini project (NAS703001TONMO711123). F.P. acknowledges funding from the German Research Foundation (DFG projects PO 1015/2-1, /3-1, /4-1), and the European Research Council (ERC Grant 724908). S.D.V.'s contribution was supported by the Icy Worlds node of NASA's Astrobiology Institute (13-13NAI7_2-0024). His part of the research was carried out at the Jet Propulsion Laboratory, California Institute of Technology, under a contract with the National Aeronautics and Space Administration.

REFERENCES

Alexander C. M. O'D. et al. (2007) The origin and evolution of chondrites recorded in the elemental and isotopic compositions of their macromolecular organic matter. *Geochim. Cosmochim. Acta, 71,* 4380–4403.

Anderson G. M. (2005) *Thermodynamics of Natural Systems, 2nd edition*. Cambridge Univ., Cambridge. 648 pp.

Bardyn A. et al. (2017) Carbon-rich dust in Comet 67P/Churyumov-Gerasimenko measured by COSIMA/Rosetta. *Mon. Not. R. Astron. Soc., 469,* S712–S722.

Běhounková M. et al. (2012) Tidally-induced melting events as the origin of south-pole activity on Enceladus. *Icarus, 219,* 655–664.

Bethke C. M. (2008) *Geochemical and Biogeochemical Reaction Modeling, 2nd edition*. Cambridge Univ., New York. 543 pp.

Beuthe M. et al. (2016) Enceladus's and Dione's floating ice shells supported by minimum stress isostasy. *Geophys. Res. Lett., 43,* 10,088–10,096.

Bouquet A. et al. (2015) Possible evidence for a methane source in Enceladus' ocean. *Geophys. Res. Lett., 42,* 1334–1339.

Bouquet A. et al. (2017) Alternative energy: Production of H_2 by radiolysis of water in the rocky cores of icy bodies. *Astrophys. J. Lett., 840,* L8, DOI: 10.3847/2041-8213/aa6d56.

Brearley A. J. (2006) The action of water. In *Meteorites and the Early Solar System II* (D. S. Lauretta and H. Y. McSween, eds.), pp. 587–624. Univ. of Arizona, Tucson.

Brown R. H. et al. (2006) Composition and physical properties of Enceladus' surface. *Science, 311,* 1425–1428.

Buchardt B. et al. (1997) Submarine columns of ikaite tufa. *Nature, 390,* 129–130.

Buchardt B. et al. (2001) Ikaite tufa towers in Ikka Fjord, southwest Greenland: Their formation by mixing of seawater and alkaline spring water. *J. Sed. Res., 71,* 176–189.

Bucher K. et al. (2015) Weathering crusts on peridotite. *Contrib. Mineral. Petrol., 169,* 52, DOI: 10.1007/s00410-015-1146-3.
Čadek O. et al. (2016) Enceladus's internal ocean and ice shell constrained from Cassini gravity, shape, and libration data. *Geophys. Res. Lett., 43,* 5653–5660.
Choblet G. et al. (2017) Powering prolonged hydrothermal activity inside Enceladus. *Nature Astron., 1,* 841–847.
Collins G. C. and Goodman J. C. (2007) Enceladus' south polar sea. *Icarus, 189,* 72–82.
Drever J. I. (1997) *The Geochemistry of Natural Waters: Surface and Groundwater Environments, 3rd edition*. Prentice Hall, Upper Saddle River. 436 pp.
Ehlmann B. L. et al. (2013) Geochemical consequences of widespread clay mineral formation in Mars' ancient crust. *Space Sci. Rev., 174,* 329–364.
Fortes A. D. (2007) Metasomatic clathrate xenoliths as a possible source for the south polar plumes of Enceladus. *Icarus, 191,* 743–748.
Fournier R. O. and Rowe J. J. (1966) Estimation of underground temperatures from the silica content of water from hot springs and wet-steam wells. *Am. J. Sci., 264,* 685–697.
Frost B. R. (1991) Introduction to oxygen fugacity and its petrologic importance. *Rev. Mineral. Geochem., 25,* 1–9.
Frost B. R. and Beard J. S. (2007) On silica activity and serpentinization. *J. Petrol., 48,* 1351–1368.
German C. R. and Seyfried W. E. (2014) Hydrothermal processes. In *Treatise on Geochemistry, 2nd edition, Vol. 8: The Oceans and Marine Geochemistry* (M. J. Mottl and H. Elderfield, eds.), pp. 191–233. Elsevier, Amsterdam.
Glein C. R. (2015) Noble gases, nitrogen, and methane from the deep interior to the atmosphere of Titan. *Icarus, 250,* 570–586.
Glein C. R. and Shock E. L. (2010) Sodium chloride as a geophysical probe of a subsurface ocean on Enceladus. *Geophys. Res. Lett., 37,* L09204, DOI: 10.1029/2010GL042446.
Glein C. R. et al. (2008) The oxidation state of hydrothermal systems on early Enceladus. *Icarus, 197,* 157–163.
Glein C. R. et al. (2015) The pH of Enceladus' ocean. *Geochim. Cosmochim. Acta, 162,* 202–219.
Haff P. K. et al. (1983) Ring and plasma: The enigmae of Enceladus. *Icarus, 56,* 426–438.
Hansen C. J. et al. (2006) Enceladus' water vapor plume. *Science, 311,* 1422–1425.
Hansen C. J. et al. (2008) Water vapour jets inside the plume of gas leaving Enceladus. *Nature, 456,* 477–479.
Hansen C. J. et al. (2011) The composition and structure of the Enceladus plume. *Geophys. Res. Lett., 38,* L11202, DOI: 10.1029/2011GL047415.
Helgeson H. C. et al. (1978) Summary and critique of the thermodynamic properties of rock-forming minerals. *Am. J. Sci., 278-A,* 1–229.
Hendrix A. R. et al. (2010) The ultraviolet reflectance of Enceladus: Implications for surface composition. *Icarus, 206,* 608–617.
Horibe Y. and Craig H. (1995) D/H fractionation in the system methane-hydrogen-water. *Geochim. Cosmochim. Acta, 59,* 5209–5217.
Hsu H-W. et al. (2011) Stream particles as the probe of the dust-plasma magnetosphere interaction at Saturn. *J. Geophys. Res.–Space Phys., 116,* A09215, DOI: 10.1029/2011JA016488.
Hsu H-W. et al. (2015) Ongoing hydrothermal activities within Enceladus. *Nature, 519,* 207–210.
Iess L. et al. (2014) The gravity field and interior structure of Enceladus. *Science, 344,* 78–80.
Ingersoll A. P. and Nakajima M. (2016) Controlled boiling on Enceladus. 2. Model of the liquid-filled cracks. *Icarus, 272,* 319–326.
Ingersoll A. P. and Pankine A. A. (2010) Subsurface heat transfer on Enceladus: Conditions under which melting occurs. *Icarus, 206,* 594–607.
Jones B. F. et al. (1977) Hydrochemistry of the Lake Magadi basin, Kenya. *Geochim. Cosmochim. Acta, 41,* 53–72.
Kelley D. S. et al. (2001) An off-axis hydrothermal vent field near the Mid-Atlantic Ridge at 30°N. *Nature, 412,* 145–149.
Kelley D. S. et al. (2005) A serpentinite-hosted ecosystem: The Lost City hydrothermal field. *Science, 307,* 1428–1434.
Kempf S. et al. (2005) Composition of saturnian stream particles. *Science, 307,* 1274–1276.
Kieffer S. W. et al. (2006) A clathrate reservoir hypothesis for Enceladus' south polar plume. *Science, 314,* 1764–1766.
Kite E. S. and Rubin A. M. (2016) Sustained eruptions on Enceladus explained by turbulent dissipation in tiger stripes. *Proc. Natl. Acad. Sci., 113,* 3972–3975.
Klein F. and Garrido C. J. (2011) Thermodynamic constraints on mineral carbonation of serpentinized peridotite. *Lithos, 126,* 147–160.
Lowell R. P. and DuBose M. (2005) Hydrothermal systems on Europa. *Geophys. Res. Lett., 32,* L05202, DOI: 10.1029/2005GL022375.
Lowenstein T. K. et al. (2014) The geologic history of seawater. In *Treatise on Geochemistry, 2nd edition, Vol. 8: Oceans and Marine Geochemistry* (M. J. Mottl and H. Elderfield, eds.), pp. 569–622. Elsevier, Amsterdam.
Malamud U. and Prialnik D. (2016) A 1-D evolutionary model for icy satellites, applied to Enceladus. *Icarus, 268,* 1–11.
Marion G. M. et al. (2012) Modeling ammonia-ammonium aqueous chemistries in the solar system's icy bodies. *Icarus, 220,* 932–946.
Matson D. L. et al. (2007) Enceladus' plume: Compositional evidence for a hot interior. *Icarus, 187,* 569–573.
Matson D. L. et al. (2012) Enceladus: A hypothesis for bringing both heat and chemicals to the surface. *Icarus, 221,* 53–62.
Matson D. L. et al. (2018) Enceladus' near-surface CO_2 gas pockets and surface frost deposits. *Icarus, 302,* 18–26.
McCollom T. M. and Shock E. L. (1998) Fluid-rock interactions in the lower oceanic crust: Thermodynamic models of hydrothermal alteration. *J. Geophys. Res.–Solid Earth, 103,* 547–575.
McKay C. P. et al. (2008) The possible origin and persistence of life on Enceladus and detection of biomarkers in the plume. *Astrobiology, 8,* 909–919.
McKinnon W. B. (2015) Effect of Enceladus's rapid synchronous spin on interpretation of Cassini gravity. *Geophys. Res. Lett., 42,* 2137–2143.
Médard E. and Kiefer W. S. (2017) Differentiation of water-rich planetary bodies: Dehydration, magmatism and water storage. In *Lunar and Planetary Science XLVIII,* Abstract #2749. Lunar and Planetary Institute, Houston.
Millero F. J. (2013) *Chemical Oceanography, 4th edition*. CRC, Boca Raton. 591 pp.
Morrill P. L. et al. (2013) Geochemistry and geobiology of a present-day serpentinization site in California: The Cedars. *Geochim. Cosmochim. Acta, 109,* 222–240.
Murray A. E. et al. (2012) Microbial life at –13°C in the brine of an ice-sealed Antarctic lake. *Proc. Natl. Acad. Sci., 109,* 20,626–20,631.
Nakajima M. and Ingersoll A. P. (2016) Controlled boiling on Enceladus. 1. Model of the vapor-driven jets. *Icarus, 272,* 309–318.
Neveu M. et al. (2015) Prerequisites for explosive cryovolcanism on dwarf planet-class Kuiper belt objects. *Icarus, 246,* 48–64.
Neveu M. et al. (2017) Aqueous geochemistry in icy world interiors: Equilibrium fluid, rock, and gas compositions, and fate of antifreezes and radionuclides. *Geochim. Cosmochim. Acta, 212,* 324–371.
Niles P. B. et al. (2013) Geochemistry of carbonates on Mars: Implications for climate history and nature of aqueous environments. *Space Sci. Rev., 174,* 301–328.
Nimmo F. et al. (2007) Shear heating as the origin of the plumes and heat flux on Enceladus. *Nature, 447,* 289–291.
Okumura F. and Mimura K. (2011) Gradual and stepwise pyrolyses of insoluble organic matter from the Murchison meteorite revealing chemical structure and isotopic distribution. *Geochim. Cosmochim. Acta, 75,* 7063–7080.
Ootsubo T. et al. (2012) AKARI near-infrared spectroscopic survey for CO_2 in 18 comets. *Astrophys. J., 752,* 15, DOI: 10.1088/0004-637X/752/1/15.
Patthoff D. A. and Kattenhorn S. A. (2011) A fracture history on Enceladus provides evidence for a global ocean. *Geophys. Res. Lett., 38,* L18201, DOI: 10.1029/2011GL048387.
Porco C. C. et al. (2006) Cassini observes the active south pole of Enceladus. *Science, 311,* 1393–1401.
Porco C. et al. (2014) How the geysers, tidal stresses, and thermal emission across the south polar terrain of Enceladus are related. *Astron. J., 148,* 45, DOI: 10.1088/0004-6256/148/3/45.
Postberg F. et al. (2008) The E-ring in the vicinity of Enceladus: II. Probing the moon's interior — The composition of E-ring particles. *Icarus, 193,* 438–454.
Postberg F. et al. (2009) Sodium salts in E-ring ice grains from an ocean below the surface of Enceladus. *Nature, 459,* 1098–1101.
Postberg F. et al. (2011) A salt-water reservoir as the source of a compositionally stratified plume on Enceladus. *Nature, 474,* 620–622.

Postberg F. et al. (2018) Macromolecular organic compounds from the depths of Enceladus. *Nature, 558,* 564–568.
Ray C. et al. (2017) Oxidation in Enceladus' ocean. Abstract P51F-08 presented at 2017 Fall Meeting, AGU, San Francisco, California, 11–15 December.
Schmidt J. et al. (2008) Slow dust in Enceladus' plume from condensation and wall collisions in tiger stripe fractures. *Nature, 451,* 685–688.
Schubert G. et al. (2007) Enceladus: Present internal structure and differentiation by early and long-term radiogenic heating. *Icarus, 188,* 345–355.
Seewald J. S. (1994) Evidence for metastable equilibrium between hydrocarbons under hydrothermal conditions. *Nature, 370,* 285–287.
Sekine Y. et al. (2015) High-temperature water-rock interactions and hydrothermal environments in the chondrite-like core of Enceladus. *Nature Commun., 6,* 8604, DOI: 10.1038/ncomms9604.
Seyfried W. E. et al. (2011) Vent fluid chemistry of the Rainbow hydrothermal system (36°N, MAR): Phase equilibria and *in situ* pH controls on subseafloor alteration processes. *Geochim. Cosmochim. Acta, 75,* 1574–1593.
Seyfried W. E. et al. (2015) The Lost City hydrothermal system: Constraints imposed by vent fluid chemistry and reaction path models on subseafloor heat and mass transfer processes. *Geochim. Cosmochim. Acta, 163,* 59–79.
Shock E. L. and McKinnon W. B. (1993) Hydrothermal processing of cometary volatiles — Applications to Triton. *Icarus, 106,* 464–477.
Shock E. L. et al. (1989) Calculation of the thermodynamic and transport properties of aqueous species at high pressures and temperatures: Standard partial molal properties of inorganic neutral species. *Geochim. Cosmochim. Acta, 53,* 2157–2183.
Smith H. T. et al. (2008) Enceladus: A potential source of ammonia products and molecular nitrogen for Saturn's magnetosphere. *J. Geophys. Res.–Space Phys., 113,* A11206, DOI: 10.1029/2008JA013352.
Spencer J. R. et al. (2006) Cassini encounters Enceladus: Background and the discovery of a south polar hot spot. *Science, 311,* 1401–1405.
Squyres S. W. et al. (1983) The evolution of Enceladus. *Icarus, 53,* 319–331.
Stähler S. C. et al. (2018) Seismic wave propagation in icy ocean worlds. *J. Geophys. Res.–Planets, 123,* 206–232.
Stolper D. A. et al. (2014) Formation temperatures of thermogenic and biogenic methane. *Science, 344,* 1500–1503.
Streit E. et al. (2012) Coexisting serpentine and quartz from carbonate-bearing serpentinized peridotite in the Samail Ophiolite, Oman. *Contrib. Mineral. Petrol., 164,* 821–837.
Thomas P. C. et al. (2016) Enceladus's measured physical libration requires a global subsurface ocean. *Icarus, 264,* 37–47.
Tillner-Roth R. and Friend D. G. (1998) A Helmholtz free energy formulation of the thermodynamic properties of the mixture {water + ammonia}. *J. Phys. Chem. Ref. Data, 27,* 63–96.
Tobie G. et al. (2008) Solid tidal friction above a liquid water reservoir as the origin of the south pole hotspot on Enceladus. *Icarus, 196,* 642–652.
Tracy R. J. and Frost B. R. (1991) Phase equilibria and thermobarometry of calcareous, ultramafic and mafic rocks, and iron formations. *Rev. Mineral. Geochem., 26,* 207–289.
Travis B. J. and Schubert G. (2015) Keeping Enceladus warm. *Icarus, 250,* 32–42.
Turcotte D. L. and Schubert G. (2002) *Geodynamics, 2nd edition*. Cambridge Univ., New York. 472 pp.
Ueda H. et al. (2016) Reactions between komatiite and CO_2-rich seawater at 250° and 350°C, 500 bars: Implications for hydrogen generation in the Hadean seafloor hydrothermal system. *Prog. Earth Planet. Sci., 3,* 35, DOI: 10.1186/s40645-016-0111-8.
Vance S. et al. (2007) Hydrothermal systems in small ocean planets. *Astrobiology, 7,* 987–1005.
Vance S. et al. (2014) Ganymede's internal structure including thermodynamics of magnesium sulfate oceans in contact with ice. *Planet. Space Sci., 96,* 62–70.
Vance S. D. et al. (2016) Geophysical controls of chemical disequilibria in Europa. *Geophys. Res. Lett., 43,* 4871–4879.
Vance S. D. et al. (2018) Geophysical investigations of habitability in ice-covered ocean worlds. *J. Geophys. Res.–Planets, 123,* 180–205.
Von Damm K. L. et al. (1985) Chemistry of submarine hydrothermal solutions at 21°N, East Pacific Rise. *Geochim. Cosmochim. Acta, 49,* 2197–2220.
Wagner W. and Pruß A. (2002) The IAPWS formulation 1995 for the thermodynamic properties of ordinary water substance for general and scientific use. *J. Phys. Chem. Ref. Data, 31,* 387–535.
Waite J. H. et al. (2006) Cassini Ion and Neutral Mass Spectrometer: Enceladus plume composition and structure. *Science, 311,* 1419–1422.
Waite J. H. et al. (2009) Liquid water on Enceladus from observations of ammonia and ^{40}Ar in the plume. *Nature, 460,* 487–490.
Waite J. H. et al. (2017) Cassini finds molecular hydrogen in the Enceladus plume: Evidence for hydrothermal processes. *Science, 356,* 155–159.
Wand U. et al. (1997) Evidence for physical and chemical stratification in Lake Untersee (central Dronning Maud Land, East Antarctica). *Antarct. Sci., 9,* 43–45.
Zolotov M. Y. (2007) An oceanic composition on early and today's Enceladus. *Geophys. Res. Lett., 34,* L23203, DOI: 10.1029/2007GL031234.
Zolotov M. Y. (2012) Aqueous fluid composition in CI chondritic materials: Chemical equilibrium assessments in closed systems. *Icarus, 220,* 713–729.
Zolotov M. Y. (2017) Aqueous origins of bright salt deposits on Ceres. *Icarus, 296,* 289–304.
Zolotov M. Y. and Fegley B. (2000) Eruption conditions of Pele volcano on Io inferred from chemistry of its volcanic plume. *Geophys. Res. Lett., 27,* 2789–2792.
Zolotov M. Y. and Kargel J. S. (2009) On the composition of Europa's icy shell, ocean, and underlying rocks. In *Europa* (R. T. Pappalardo et al., eds.), pp. 431–457. Univ. of Arizona, Tucson.
Zolotov M. Y. and Postberg F. (2014) Can nano-phase silica originate from chondritic fluids? The application to Enceladus' SiO_2 particles. In *Lunar and Planetary Science XLV,* Abstract #2496. Lunar and Planetary Institute, Houston.